Complex-shaped magnetic 3D cell-based structures for tissue engineering

Lúcia F. Santos[1], *A. Sofia Silva*[1,*], *João F. Mano*[1,*]

[1]CICECO-Aveiro Institute of Materials, Department of Chemistry, University of Aveiro Campus de Santiago, 3810-193 Aveiro, Portugal

Corresponding authors: sofiamsilva@ua.pt; jmano@ua.pt

Abstract

The use of cells as building blocks for tissue engineering purposes has been a matter of research in the recent years. Still, the fabrication of complex-shaped 3D-like constructs using living-based materials is hampered through the difficulty in recapitulating the mechanical properties of the native tissues. In an attempt to develop robust tissue-like constructs, it is herein proposed the fabrication of complex-shaped magnetic cells sheets (CSs) with improved mechanical properties for bone TE. Hence, magnetic CSs with versatile shapes and enhanced mechanical performance are fabricated using a pre-osteoblast cell line (MC3T3-E1) through an universal approach that relies on the design of the substrate, cell density and magnetic force. Results show that such magnetic CSs exhibit a Young's modulus similar to those encountered in the soft tissues. The construction of stratified CSs is also explored using MC3T3-E1 and adipose-derived stromal cells (ASCs). The role of the pre-osteoblast cell line on ASCs osteogenesis is herein investigated for the first time, in layered scaffold-free structures. After 21 days, the level of osteogenic markers in the heterotypic CS (MC3T3-E1:ASCs) is significantly higher than in the homotypic one (ASCs:ASCs), even in the absence of osteogenic differentiation factors. These evidences open new prospects for the creation of mechanically robust, complex, higher-ordered and completely functional 3D cell-based materials that better resemble the native environment of *in vivo* tissues.

Statement of Significance

Materials science, matrix biology and tissue engineering (TE) have been increasingly combined to generate biomimetic materials able to recapitulate the complexity, strength and longevity of natural tissues. By providing magnetic cells as building blocks, this work proposes the fabrication of mechanically strong and complex-shaped 3D-like tissues using magnetic-force based tissue engineering (Mag-TE) in a simple, cost-effective and time-saving fashion. A plethora of organized tissues could be created using such universal approach that relies on the design of the substrate, cell density and magnetic force. Such cell-based constructs are able to resemble the complex environment of native tissues and simulate their mechanical performance, offering potential applications for the production of *in vitro* disease models or implantable structures for tissue/organ repair or regeneration.

Keywords: Complex-shape, magnetic cell sheet, mechanical behavior, tissue engineering, robustness

1. Introduction

Tissue engineering (TE) aims to generate *in vitro* biological tissues and organs to replace lost or compromised tissues.[1] In this sense, TE approaches have been focused on the creation of microenvironments that promote the regeneration of the injured site through the interaction of materials, cells and growth factors.[2] Therefore, natural and synthetic biomaterials have been serving as scaffolds for biologically active components (cells) in order to define an artificial *in vivo* milieu with complex and dynamic interactions that regulate stem cells, mimicking their natural cellular microenvironment, and consequently leading to tissue formation.[3–5] Nevertheless, the possible strong inflammatory responses that are induced upon scaffold biodegradation, the limited diffusion of nutrients that promote a necrotic core and even the use of isolated cell suspension that deprive cells of their endogenous extracellular matrix (ECM), results in the failure of tissue reconstruction and, therefore, unsatisfactory regeneration.[6]

Additionally, the complex, well-organized and hierarchical architecture of tissues and organs is not fulfil by traditional TE approaches. Flat tissues, tubular structures, hallow, nanotubular, viscous organs and complex solid organs exhibit single features that became unique challenges in TE.[7,8] In such way, materials science, matrix biology and TE have been increasingly combined to generate a new class of biomimetic materials to closely mimic critical aspects of natural tissue regarding its physical and chemical properties. In this sense, scaffold-free TE has emerged as a powerful strategy using multicellular building blocks like spheroids, tissue strands and cell sheets (CSs) that are able to produce larger cohesive tissue constructs and produce ECM, that is essential to fabricate functional tissues.[6,9] In particular, CS technology has been getting momentum due to their ability to fabricate more functional, complex, and thicker heterogeneous tissues.[10] Such expertise allows the construction and harvesting of intact sheet-like cells, keeping their naturally formed cellular networks.[11–14] Thermo-responsive methodology is the most explored cell harvesting mechanism in which sheets of cells are recovered by simply changing the temperature. Nevertheless, such strategy exhibits several constraints including the high cost, alteration of cellular activity, low mechanical strength and restrains in tissue replacement.[15] Moreover, due to the complexity of organs and tissues, the fabrication of *in vivo*-like 3D constructs using CS technology may be a challenge. The development of heterotypic and stratified 3D tissue is normally achieved by individual stacking of previously formed CS monolayers. Nevertheless, such strategy could hamper the establishment of cell-cell interactions between the two different cell cultures, and hinder a controlled spatial positioning of target cells, compromising the natural stratification of the 3D tissue.[16]

In the light of such events, magnetic-force based tissue engineering (Mag-TE) has been explored in order to produce more complex CSs through the combination of magnetic force with CS technology, enabling the easier manipulation of those cells. [10,17] In fact, Mag-TE has been implied in the production of complex tissues that are not easily achieved by

conventional cell culture or co-culture methods such as 2D and 3D cell layers, tubular structures and 3D ordered assemblies consisting of several cell types.[17,18] Thus, magnetic CSs have been investigated in the regeneration of distinct tissues including skeletal and cardiac muscle,[14,16] bone[19] and angiogenesis,[20–22] emphasizing the ability of this technology over artificial synthetic scaffolding materials for a wide range of tissues. Recently, Mag-TE has shown outstanding results in the development of hierarchical 3D cohesive tissues in a simple, one-pot, cost-effective and time-saving manner, allowing the fabrication and manipulation of tissue-like constructs aided by a magnetic force.[10,23] In fact, such 3D construct revealed to be effective in stimulating *in vitro* osteogenesis and triggering the recruitment of blood vessels with empowering pre-angiogenic potential.[10] Nevertheless, the geometry, complexity and strength of the tissue-constructs still poorly-explored, which could compromise the proper function of these living materials. Tissue engineered constructs should resemble the *in vivo* structural and mechanical properties of the native tissues to assure their functionality and integration within the host.[24]

In light of such events, our group aims to investigate the ability of creating versatile and robust magnetic CSs, while guarantying the natural architecture of living tissues. Hence, the current work aims, in a first approach, at developing complex and robust magnetic membranes based exclusively on the type of magnet and substrate applied. For the purpose, mouse pre-osteoblastic cells (MC3T3-E1) were used to create different shapes of magnetic cell tissue. The robustness of such cell-dense like tissue will be validated by accessing their mechanical performance as well as by the deposition of ECM. In fact, the mechanical performance of cell-based tissue constructs was herein explored for the first time. Moreover, as a proof-of-concept, to demonstrate the ability of this technology in creating heterotypic 3D cell connected tissue, adipose derived stromal cells (ASCs), previously labelled with magnetic iron oxide nanoparticles (MNPs), were seeded on top of the magnetically labelled MC3T3-E1 CS enabling tissue stratification. We hypothesized that such approach could prompted the fabrication of cell-

based constructs to create stratified cell-dense tissues for bone TE. In fact, to the best of our knowledge, the ability of pre-osteogenic linage to modulate the osteogenic differentiation of stromal cells was never tested in such layered scaffold-free structures. We expect that the methodology herein described could be further extended for the regeneration of a wide plethora of organized tissues, enabling the creation of a living-based construct with biomimetic mechanical properties.

2. Materials and methods

2.1. Materials

All chemicals were purchased from Sigma-Aldrich and employed as received, unless otherwise specified.

2.2. Synthesis and Characterization of Magnetic Nanoparticles

Magnetite nanoparticles were synthesized as previously established by the group.[25] Briefly, Fe_3O_4 MNPs nanoparticles were synthesized by the co-precipitation reaction of ferrous ($FeCl_2 .4H_2O$) and ferric ($FeCl_3 .6H_2O$) salts at 60°C, in a nitrogen atmosphere and in the presence of ammonium hydroxide (NH_4OH). Then, MNPs surface was modified with (3-aminopropyl)triethoxysilane (APTES) by a silanization reaction and washed with water, and ethanol followed by freeze-drying. Later on, the nanoparticles were conjugated with rhodamine B isothiocyanate as previously established.[10,25] For this purpose, Fe_3O_4 –APTES MNPs were dispersed in ethanol at 5 mg mL^{-1} and then, rhodamine B (RhodB) (2.5 mg mL^{-1}) was added at RT, overnight. The modification of the MNPs with APTES was accessed by attenuated total reflectance (ATR-FTIR) by using a Bruker Tensor 27 spectrometer, as described in our previous report.[10].

2.3. Evaluation of the Fe_3O_4 – APTES RhodB-MNPs Stability

The stability of RhodB-MNPs was investigated by scanning the fluorescence of RhodB on cell culture medium and dPBS (pH=7.4). Briefly, the samples were immersed and subsequently stirred in a shaking water bath at 60 rpm and 37ºC. After 1, 3, 7, 14 and 21 days, the fluorescence spectrum was peaked at an excitation wavelength of 556 nm and 627 nm of emission using a spectrofluorometer (FP-8300, JASCO, USA).

2.4. Cell culture and *In vitro* cellular uptake of RhodB-MNPs

MC3T3-E1 cell line (ATCC® CRL-2593) and human ASCs (ATCC® PCS-500-011™) were cultured in α-MEM (minimum essential medium, ThermoFisher Scientific), supplemented with fetal bovine serum (FBS, 10%, ThermoFisher Scientific) and penincilin-streptavidivin (1% v/v, ThermoFisher Scientific). The co-location of RhodB-MNPs was visualized in both MC3T3-E1 cell line and ASCs. Firstly, cells were seeded at density of 2.4 x 10^6 cells cm^{-2} in 8-well cell culture slides and cultured for 24 h at 37 °C and 5% CO_2 in a humidified atmosphere, followed by a 4 h incubation with RhodB-MNPs at 1 mg mL^{-1}. Lastly, cells were washed with PBS and subsequently fixed in formalin 10% (v/v) at RT during 15 min. After the incubation of the cells with Triton X100 (0.1% (v/v), in dPBS) during 5 min at RT, the cells were incubated with Flash Phalloidin Green 488 (1:100 in dPBS) at RT for 45 minutes and then counterstaining with DAPI (1:1000 in dPBS) for 5 min at RT. Finally, the cells were visualized by fluorescence microscopy (Carl Zeiss Microscopy GmbH) and using ZEN v2.3 blue edition.

2.5. Fabrication of homotypic and heterotypic magnetic CSs

Prior to cell seeding, MC3T3-E1 and ASCs were incubated during 30 minutes at 37 °C with the lipophilic dyes 3,3′-dioctadecyloxacarbocyanine perchlorate (DIO, green) and 1,1'-Dioctadecyl-3,3,3',3'-Tetramethylindodicarbocyanine (DID, purple), respectively (1mL, 2μM per 1× 10^6 cells), . Then, the labeled cells were seeded at the cell density of 2.4 × 10^6 cm^{-2} and

cultured during 24 h at 37 °C and 5% CO_2 in a humidified atmosphere, followed by a 4h incubation with RhodB MNPs (1 mg mL^{-1}). Later on, the cells were harvested using TrypLE™ Express solution at 37 °C for 5 min and centrifuged at 300 g. In order to obtain CSs with flat and circular shapes, the magnetically labelled cells were transferred to ultralow-attachment 24, 48 or 96-well plates, previously treated with alginate (2% w/v) for 30 min. To provide magnetic force, commercial neodymium rod magnets (strength of 108N and standard N41 magnetization, Supermagnet) were placed at the bottom of the reverse side of the ultralow-attachment plate. The ability to create more complex structures was investigated through the fabrication of CSs with diverse shapes based on the type of magnet, substrate and cell density. For the purpose, commercial neodymium magnets with ring and concave shapes (strength of 73.5 N and standard N42 magnetization, Supermagnet) were used. Briefly, the magnetically labelled cells (MC3T3-E1 cell line) were transferred to an Eppendorf and then the magnets were placed around (ring shape) and at the bottom of (concave shape) the Eppendorf.

Heterotypic magnetic CSs were created by labelling each cell phenotype as described in the previous section. After 24 h, the second cell phenotypic (ASCs) was added to the homotypic circular MC3T3-E1 CS, that was previously assembled. The CSs with a double conformation were cultured during 7, 14 and 21 days in α-MEM medium with or without osteogenic differentiation factors - dexamethasone (10 nM), ascorbic acid (50 μg mL^{-1}) and β-glycerophosphate (10 mM). Labelled cells in both homotypic and heterotypic magnetic CSs were visualized under fluorescence microscopy (Carl Zeiss Microscopy GmbH) and processed using ZEN v2.3 blue edition.

2.5.1. Characterization and mechanical behaviour of the developed CSs

The morphology of CSs for all conditions was visualized by SEM (S4100, Hitachi, Japan. Briefly, the samples (n=2) were washed with PBS, followed by an incubation of 15 min with

formalin (10% v/v). Then, the samples were dehydrated in an increasing gradient of ethanol and gold-sputter coated using an accelerating voltage of 25 kV.

The mechanical behavior of the homotypic CS with the MC3T3-E1 cell line was investigated (n=5 independent replicas) was characterized through the tensile testing (MMT-101N, Shimazdu Scientific Instruments, Japan) with a load cell of 100 N. Briefly, ring shape CSs were cut to display a ribbon-like conformation and then, the samples were clamped in the tensile testing machine. Tensile testes were carried out with a gauge length of 3 mm and a loading speed of 1 mm min^{-1}. The cross-section of the CS was measured using SEM images. For each sample, the load versus cross-head displacement data from initial until rupture load was measured using a PC data acquisition system connected to the tester. Resulting stress-strain curves allowed to determine the ultimate tensile strength (UTS), elongation at break, and Young's modulus of the CSs.

2.6. Histological and immunohistochemical analysis of CSs

Prior to staining, the heterotypic CSs were fixed using formalin 10% (v/v) at RT for 15 min. After the permeabilization of the CSs with Triton X (0.1% v/v) during 5 min at RT, the CSs were incubated for 1h at RT with 5 % (v/v) FBS/dPBS. Then, the samples were immersed for 3 h at RT with the primary antibody anti-rabbit human vinculin (1:50 in 5 % FBS/dPBS, Invitrogen). Subsequently, the secondary antibody anti-rabbit AlexaFluor 594 (1:400 in 5% FBS/dPBS) was added to the samples during 1h at RT. Lastly, the CSs were incubated with Flash Phalloidin Green 488 (1:100 in dPBS) at RT for 45 min and counterstained with DAPI (1:1000 in dPBS) during 5 min at RT. At the end, the CSs were visualized by confocal microscopy LSM 880, ZEISS) and processed using ZEN v2.3 blue edition and Imaris Biteplane. Heterotypic CSs cultured during 21 days at basal and osteogenic conditions were also visualized in histological sections. After the fixation of the samples with formalin (10% v/v), the CSs were

routinely processed and embedded in paraffin. Then, sequential sections of 5 µm thickness were produced in adhesive slides to the Masson Trichrome and Van Kossa staining. Expression of osteocalcin, lamin A and CD44 were also visualized in the histological cross-sections. Firstly, the samples were treated with TE buffer (10 mM Tris/1 mM EDTA, pH 9) for 35 min at 95–98 °C for antigen retrieval. Then, the sections were incubated during 3 h with mouse anti-osteocalcin (1:200 in 5 % FBS/dPBS, Biolegend), rabbit anti-Lamin A (1:200 in 5 % FBS/dPBS, Biolegend), FN monoclonal antibody (FN-3) Alexa Fluor 488 (1:100 in 5 % FBS/dPBS, Thermofisher), FITC anti-human CD44 primary antibodies (1:200 in 5 % FBS/dPBS, Biolegend) and rabbit anti-collagen IV antibody (1:400 in 5% FBS/dPBS, Abcam). Lastly, the samples were incubated with Alexa Fluor 647-labeled chicken anti-rabbit (1:400 in 5 % FBS/dPBS, Invitrogen) for anti-lamin A, AlexaFluor 488 Goat anti- mouse (1:400 in 5 % FBS/dPBS, Invitrogen) for anti-osteocalcin and AlexaFluor 594 Donkey anti-rabbit (1:400 in 5 % FBS/dPBS, Invitrogen) during 1h at RT. For all conditions, the histological sections were incubated with DAPI (1:500 in dPBS, Sigma) at RT for 5 min. At the end, the CSs were visualized using a fluorescence inverted microscope (AxioImager Z1, Zeiss). Statistical differences between heterotypic CSs cultured in basal or osteogenic evidenced in the histological cuts were analyzed using Image J software.

2.7. Cell viability

The survival of the cells in MC3T3-homotypic CS, ASCs-homotypic CS and heterotypic CSs was investigated through a live-dead fluorescence assay by following the manufacturer's recommendations (ThermoFisher Scientific) at 7, 14, and 21 days of culture. After washing the samples with PBS, the CSs were incubated with the kit components during 20 min at 37 °C. Finally, the samples were analyzed by fluorescence microscopy (Axio Imager 2, Zeiss).

2.8. Quantification of Mitochondrial Metabolic Activity

Mitochondrial metabolic activity was accessed through an MTS colorimetric assay (CellTiter96® AQueous one solution cell proliferation assay, Promega) according to manufacturer's recommendations. Briefly, the reagent kit (120 µl per well) was incubated with the samples (n=3) for 4h at 37 °C and then, the absorbance was determined at 490 nm using a microplate reader (Synergy HTX, BioTek Intruments, USA).

2.9. Quantification of the Cell Proliferation

Firstly, the cell lysis was performed by resuspending the CSs (n=3) in Titron 100X (2 % v/v/ in ultra-pure sterile water) at 37 °C for 1 h. The samples were stored at −80 °C until further use. Then, the lysate DNA content was determined with Quant-iT™ PicoGreen™ dsDNA Assay Kit (Invitrogen™) according to the manufacturer's instructions. To guaranty that only DNA content would be quantified, the MNPs were firstly magnetically separated with the aid of a neodymium magnet. A standard curve for DNA analysis was generated with the provided the standard DNA solution. Lastly, the samples were incubated at RT for 10 min and the fluorescence intensity was determined at an excitation wavelength of 485/20nm and 528/20nm of emission using a microplate reader (Synergy HTX, BioTek Intruments, USA).

2.10. Analysis of osteogenic differentiation of the CSs

The role of MC3T3-E1 in the osteogenic differentiation of ASCs was evaluated in culture medium with and without osteogenic differentiating factors (dexamethasone, ascorbic acid and β-glycerol phosphate). Homotypic CSs composed of ACSs and MC3T3-E1 were used as controls. All CSs were incubated for over a period of 21 days.

2.10.1. Quantification of ALP Activity

The cell lysates were also analyzed for the quantification of the alkaline phosphatase activity (ALP) by measuring the released p-nitrophenol (4NPhP). Briefly, 75 µL of 4NPhP solution (2

mg mL^{-1} in) in 1M diethanolamine buffer were added to 25 μL of each sample. After 45 min at 37 °C in dark, the reaction was stopped with 80 μL of a NaOH (2 M) and EDTA (0.2 mM) solution. Lastly, the enzyme activity was determined at 405 nm using a multiplate reader (Synergy HTX, BioTek Intruments, USA). The value was normalized against the CS area. A standard curve with a range of 4NPh concentration was used as reference (0; 15×10^{-6}; 30×10^{-6}; 50×10^{-6}; 75×10^{-6}; 95×10^{-6} M in diethanolamine buffer).

2.10.2. Osteopontin Immunostaining

The expression of osteopontin was determined in both homotypic and heterotypic CSs, previously labelled with DIO (MC3T3-E1) and DID (ASCs). After 7, 14 or 21 days of culture, the CSs were fixed in formalin (10% v/v) at RT during 15 min. Firstly, the samples were immersed in Triton X (0.1% v/v, in dPBS) at RT for 5 min. Then, the CSs were incubated with 5 % (v/v) FBS/dPBS at RT for 1 h. Subsequently, the primary mouse anti-human osteopontin antibody (1:100 in 5% FBS/dPBS, Biolegend, Taper) was added to the samples. After 3h, the CSs were incubated with the secondary anti-mouse Alexa Fluor 555 antibody (1:400 in 5 % FBS/dPBS) for 1h in dark at RT. Lastly, all the samples were counterstained with DAPI (1:1000 in dDPBS) during 5 min in dark at RT and visualized by fluorescence microscopy (Carl Zeiss Microscopy GmbH) and using ZEN v2.3 blue edition.

2.10.3. Quantification of Cytokines

After 21 days of culture, the culture medium from the MTS, DNA and ALP activity assays was collected and stored at -80°C until further use.

The expression of osteopontin, osteocalcin, BMP-2 and VEGF was quantified through the commercially available Human Osteopontin (Abcam), Osteocalcin (Abcam), BMP-2 (Invitrogen) and VEGF (Abcam) ELISA Kits, respectively. Lastly, the absorbance of the

samples was determined at 450 nm using a microplate reader (Synergy HTX, BioTek Intruments, USA).

2.10.4. In vitro biomineralization analysis of the CS

After 7, 14 and 21 days of culture, the *in vitro* mineralization of CSs was accessed for both basal and osteogenic culture conditions using the OsteoImage™ Assay. For this purpose, the CSs were incubated with the OsteoImage™ staining reagent (1:100 v/v) during 30 min at RT. Then, the samples were counterstained with DAPI (1:1000 in dDPBS) during 5 min in dark at RT and visualized by fluorescence microscopy (Carl Zeiss Microscopy GmbH). The deposition of hydroxyapatite nodules was also visualized by SEM. Briefly, the CSs were carbon-coated and analyzed by Energy dispersive X-ray spectroscopy (EDS) (QUANTAX 400, Bruker) at an electron in intensity of 15 kV (SU-70, Hitachi).

2.11. Statistical Analysis

All the results were stated as mean ± standard error. GraphPad Prism software (GraphPad Software Inc., version 7.0) was used for the statistical analysis by two-way ANOVA following the Bonderronu pos-hoc test, with a significance level set at $P < 0.05$.

3. Results

3.1. Cell Sheet Fabrication and Characterization

RhodB-MNPs were produced and characterized according well-established protocols of the group (**Figure 1A**).[10,25] Prior to CSs fabrication, the stability of the magnetic nanoparticles modified with Rhodamine B (RhodB-MNPs) was confirmed in dPBS and culture medium over a course of 21 days (**Figure S1**). Moreover, RhodB-MNPs were successfully uptaken by MC3T3-E1 and ASCs as corroborated in **Figure S2**. Afterwards, homotypic and heterotypic magnetic CSs were prepared as described elsewhere[10] and as illustrated in **Figure 1B**.

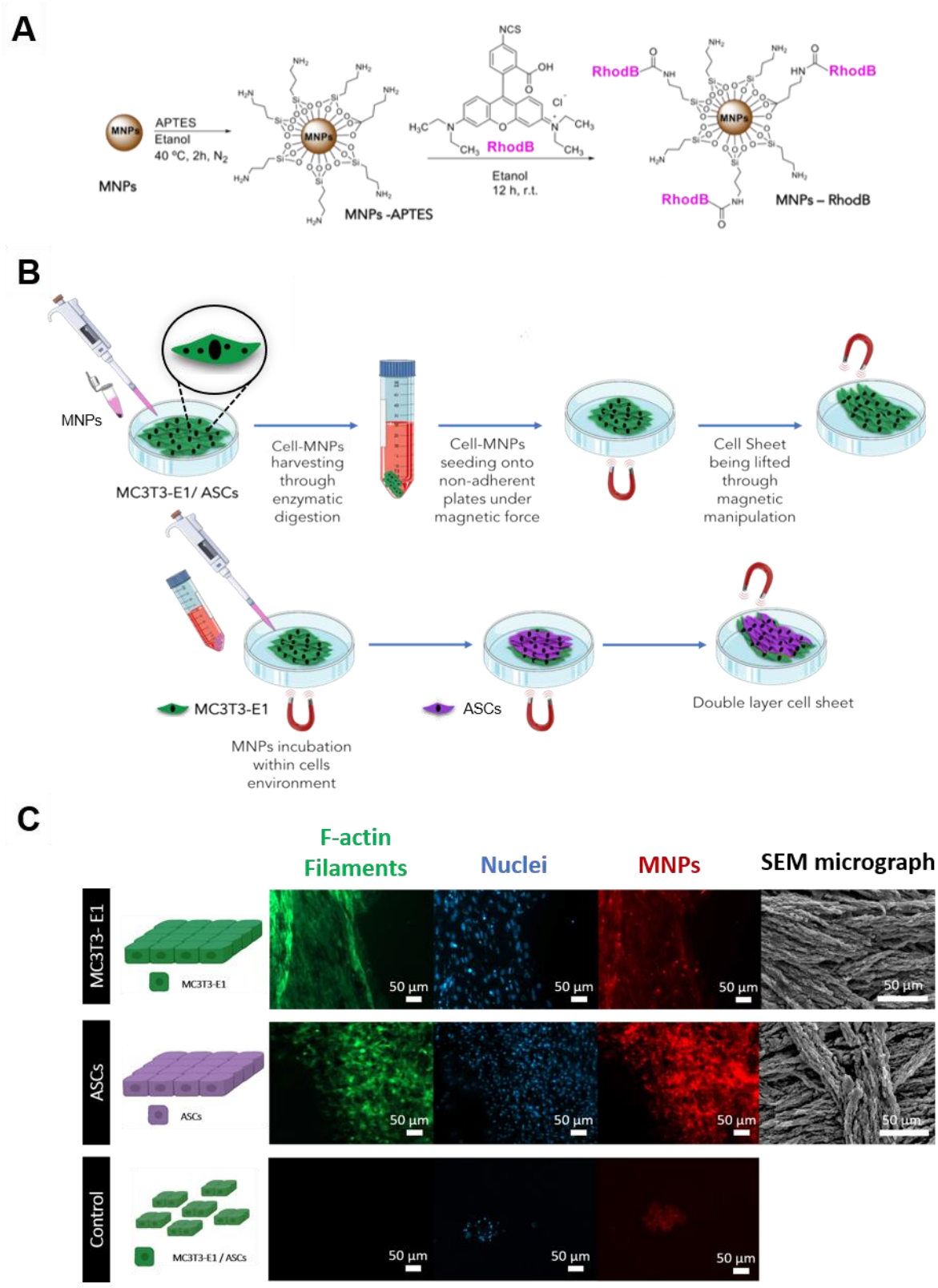

Figure 1. Development of CSs using Mag-TE. **A**. Schematic representation of the functionalization of MNPs used in the fabrication of CSs. **B**. Schematic illustration of the proposed approach for the development of magnetic CSs; **C**. Fluorescence and SEM images of the fabricated homotypic CSs using MC3T3-E1 and ASCs. Same cell assembly procedure without the aid of magnet was used as control and a representation of the MC3T3-E1 cell assembly is demonstrated.

3.1.1. Homotypic Cell Sheet

Initially, ASCs and MC3T3-E1 cells were used for the development of homotypic CSs. As demonstrated in **Figure 1C**, homotypic CSs were successfully produced with the aid of the magnetic field. In the absence of the magnet only a few aggregates were formed, and no cell-cell interaction was denoted.

To further demonstrate the versatility of this approach in creating distinct and functional tissues, CSs with diverse shapes were developed based on the type of the magnet, substrate and cell density. As a proof-of concept, MC3T3-E1 cells were used to produce robust CSs with circular, ring and concave shapes. **Figure 2A** displays the fluorescence images of such shaped CSs, corroborating the deposition of ECM within the well-defined structures. Additionally, CSs' cell density, thickness and morphology were also investigated along time (7, 14 and 21 days) in the MC3T3-homotypic CSs through SEM (**Figure S3**, **Figure S4**). As hypothesized, the CS thickness and robustness increased with the cell density.[26] Nevertheless, the thickness of the CSs decreased along time (**Figure S3**), thus suggesting tissue confinement and therefore, the stratification of the CS.

3.1.2. Mechanical properties

MC3T3-homotypic CSs were used to evaluate their mechanical behavior and robustness. The tests were performed using a tensile mode - see **Figure 2B**. Representative conventional stress–strain curve and the respective values of Young's modulus, ultimate tensile strength and maximum extension are shown in **Figure 2C** and **D**. Herein, CSs presented a maximum extension of 0.55 ± 0.06, a Young's modulus of 22 ± 5 kPa and an ultimate tensile strength of 10 ± 3 kPa.

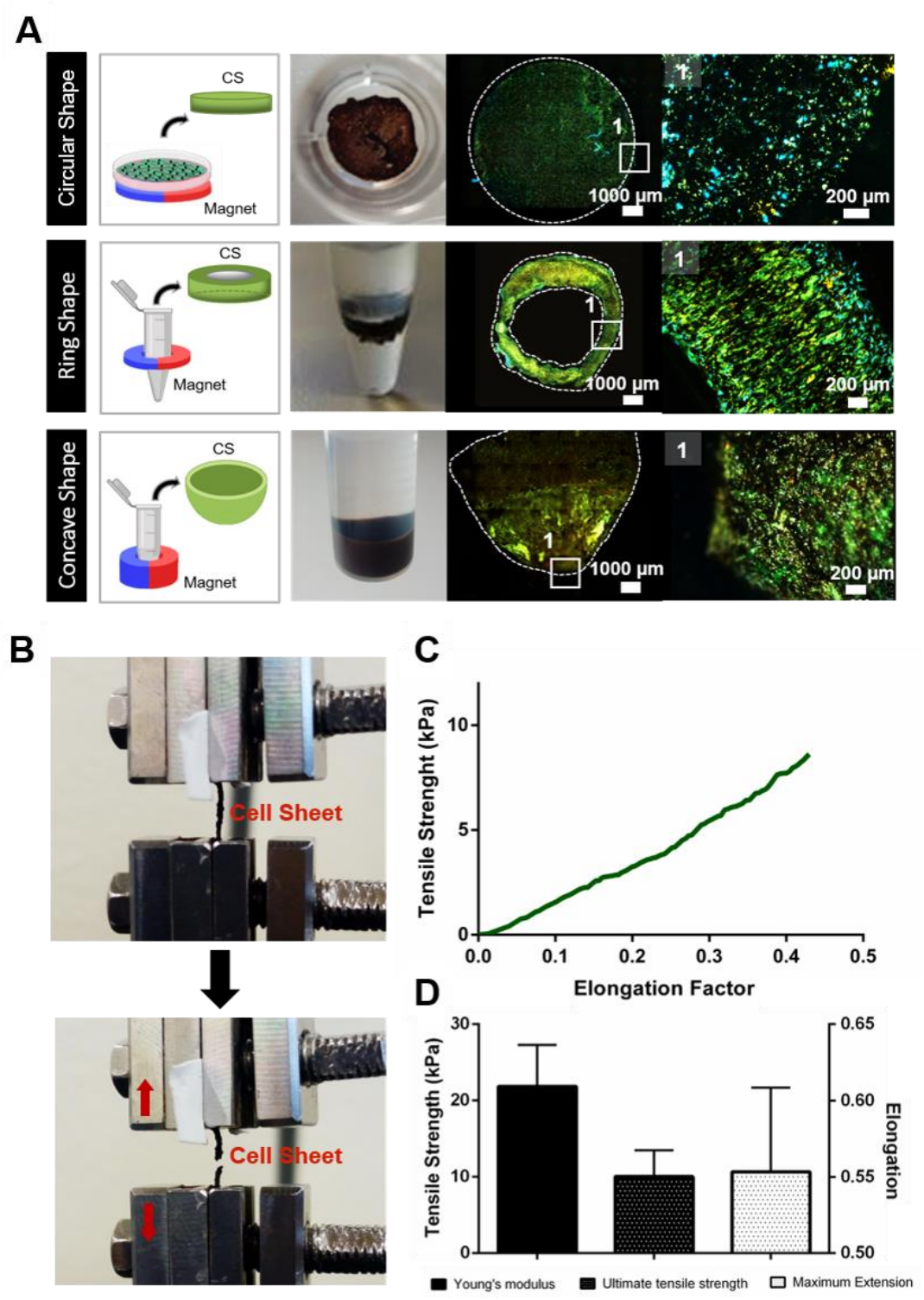

Figure 2. A. Development of versatile MC3T3-homotypic CSs with different shapes, including circular, ring and concave shaped structures. **B.** Photographs of the MC3T3-homotypic CSs during the tension assay performed to evaluate their mechanical behavior; **C.** Representative conventional tensile strain–stress curve of the MC3T3-homotypic CS; **D**. Mechanical performance of the developed CSs – Young's modulus, Ultimate Tensile Strength and Maximum Extension.

3.1.3. Heterotypic Cell Sheet

The major challenge in TE prevails on the construction of highly controlled constructs able to fil distinct defects. In an attempt to investigate the ability to create heterotypic stratified cell-dense like tissue, magnetic CSs comprising MC3T3-E1 and ASCs were fabricated. The double layer CS conformation was built by seeding a suspension of magnetically labelled ASCs on the top of a previously assembled MC3T3-homotypic CS. The CS assembly was corroborated by confocal microscopy (**Figure 3A** and **Figure S5**) with ASCs displayed in purple and MC3T3-E1 represented in green. Cell-cell interactions throughout the CS construct were confirmed by the vinculin staining (**Figure 3B**).

3.2. Viability, metabolic Activity and Cell Proliferation

Heterotypic CSs in both basal and osteogenic culture media showed increased metabolic activity and DNA content up to 14 days of culture. Moreover, for all the conditions the majority of the cells remained viable after 21 days of culture (**Figure S6**). On the other hand, the homotypic CSs conformations (ASCs CSs or MC3T3-E1 CSs) exhibited lower metabolic activity (**Figure 3C**) after 21 days of culture, suggesting a compromised viability along time for the monolayer CS conformations.

3.3. Evaluation of the *in vitro* osteogenic differentiation of the Magnetic CSs

To demonstrate the cells interactions within the CSs, we investigated the ability of MC3T3-E1 to induce the osteogenic differentiation of ASCs through the evaluation of alkaline phosphatase (ALP) activity, mineralization and cytokines detection.

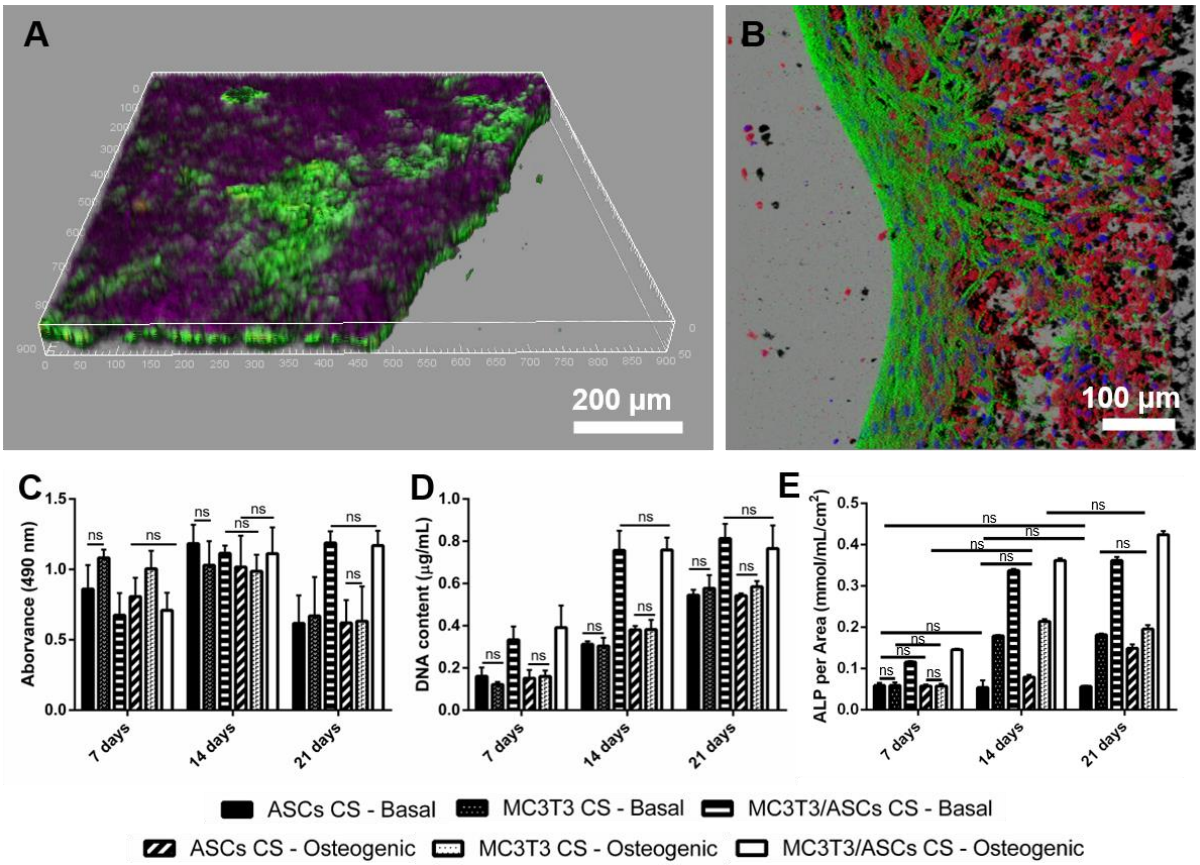

Figure 3. Construction of stratified heterotypic CSs. **A**. Confocal microscopy image of the 3D stratified CS with a double layer conformation: ASCs CS (purple) on the top of MC3T3-E1 CS (green); **B**. Confocal microscopy image of the heterotypic CS cultured for 7 days. The presence of vinculin (in red) in the actin cytoskeleton (in green) confirmed the cell-cell and cell-matrix junctions. Cell nuclei are depicted in blue (DAPI). **C**. Cell metabolic activity determined by MTS colorimetric assay, **D**. Cell proliferation by DNA quantification, and **E**. Alkaline phosphatase (ALP) activity normalized by the CS area. All results were significantly different unless marked with ns ($p > 0.05$).

3.3.1. Quantification of the ALP activity

Since enhanced levels of ALP activity are associated with the mineralization of bone,[27] we envisage that early cell differentiation had occurred on heterotypic CSs and MC3T3-homotypic CSs. The ASCs-homotypic CS presented an increment on ALP activity in the presence of the osteogenic differentiation factors after 21 days (**Figure 3E**). On the other hand, in basal conditions (i.e., without the supplementation of osteogenic factors such as dexamethasone, ascorbic acid and β-glycerol phosphate), ASCs-homotypic CSs do not show any increment on the ALP activity. The hypothesis that MC3T3-E1 could induce ASCs differentiation in

osteogenic progenitor cells was corroborated through the increment of the ALP activity in the heterotypic CS even in basal conditions. We demonstrated that within the CSs, MC3T3-E1 and ASCs can interact in such way that leads to diffusion of signaling molecules essential for the osteogenic differentiation of stromal cells. In fact, the heterotypic CSs (MC3T3-E1/ASCs) showed higher expression of ALP (normalized by area) when compared to MC3T3-homotypic CSs, which supports our initial hypothesis that MC3T3-E1 cell line has a positive role over the ASCs osteogenic differentiation. As expected, the addition of osteogenic factors prompted to even higher cell differentiation.

3.3.2. Osteopontin Expression

Osteopontin represents one of the most-studied protein in bone matrix, playing a critical role in the maintenance of bone structure.[27] To substantiate the synergic behavior between MC3T3-E1 and ASCs, and attest that our heterotypic CS could be further use for bone regeneration purposes, we have explored the presence of osteopontin in both homotypic and heterotypic CSs through an immunofluorescence assay. As anticipated, an earlier osteopontin detection was evidenced for the heterotypic CS in osteogenic conditions after 14 days of culture (**Figure 4**), corroborating the results obtained through the ALP activity. Nevertheless, after 21 days, the osteopontin staining could be depicted in both culturing conditions (even in basal media), suggesting the osteogenic induction of MC3T3-E1 over ASCs. In fact, the presence of osteopontin was more evident in heterotypic CS when compared to the MC3T3-homotypic CS (**Figure S7**). As expected, the ASCs-homotypic CS cultured under basal conditions (no osteogenic supplementation), did not exhibit osteopontin expression (**Figure S8**). The heterotypic-CS showed an enhanced osteopontin expression when compared to the ASCs-homotypic CS (**Figure 4**). Additionally, SEM micrographs were collected from all conditions to validate the cohesion of the developed tissue constructs.

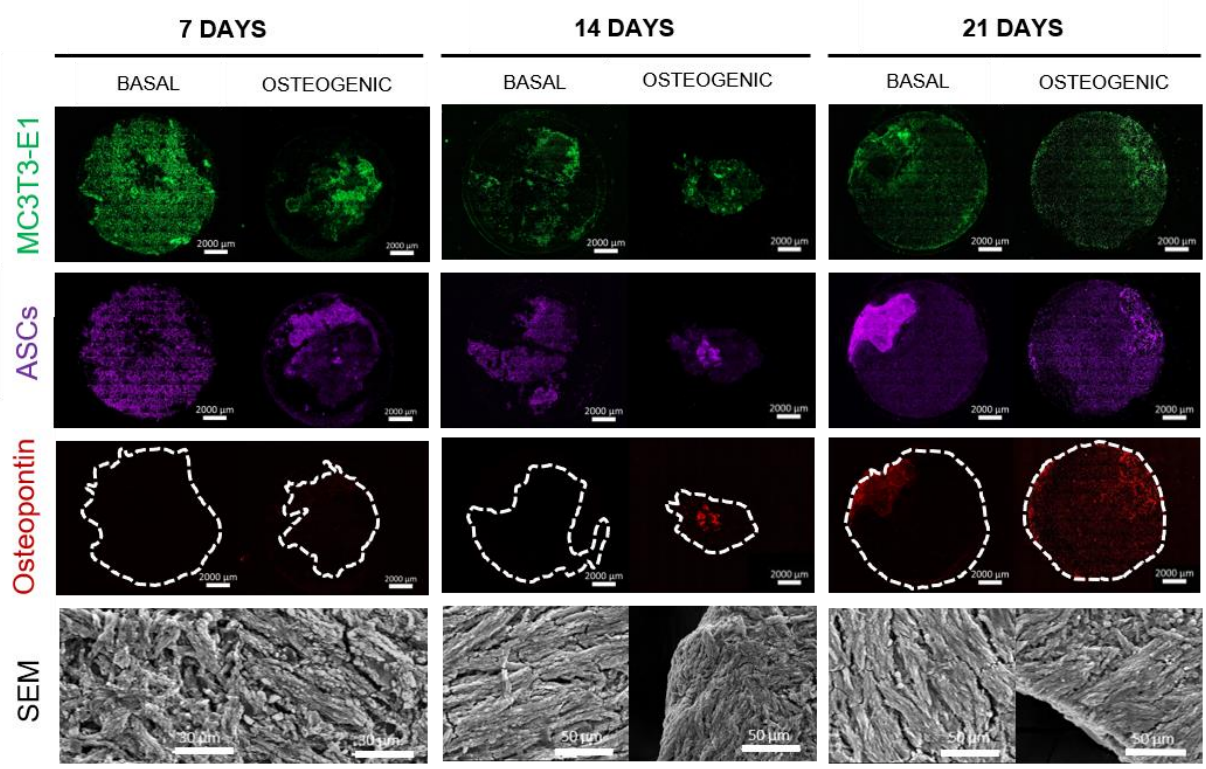

Figure 4. Immunofluorescence of heterotypic CSs after 7, 14 and 21 days of culture in basal and osteogenic media: MC3T3-E1 (green), ASCs (purple) and osteopontin (red). SEM micrographs corroborate the integrity of the developed CSs (bottom panel).

3.3.3. Biomineralization Assessment

The biomineralization of 3D constructs has been investigated in TE to attest the formation of bone-like tissues.[28–30] In the light this, we have also investigated the deposition of hydroxyapatite-like minerals on both homotypic and heterotypic CSs, since hydroxyapatite is chemically similar to the inorganic component of bone. For this purpose, the mineralization of CSs was accessed through energy dispersive X-ray spectroscopy (EDS) (**Figure 5B**) and an OsteoImage^{TM} assay (**Figure 5C**).

The results supported both ALP and osteopontin findings with increased hydroxyapatite deposition overtime in both culturing conditions of the heterotypic CSs (MC3T3-E1/ASCs). The Ca/P ratio reached the maximum value at 21 days under osteogenic supplementation (1.41). As expected, a small delay was evidenced for the heterotypic CSs cultured without osteogenic supplementation (1.12).

The results suggested the formation of bone-like tissue in both culturing conditions with an enhanced deposition of hydroxyapatite-like minerals, and a Ca/P ratio similar to native apatite minerals in bone (1.67).[31,32] The deposition of hydroxyapatite minerals was also supported by SEM micrographs. Minerals with larger sizes and more defined structures were obtained after 21 days, corroborating the findings of EDS quantification. The hydroxyapatite deposition was also visualized through an OsteoImage^{TM} Assay, attesting higher mineralization in the heterotypic CS. As expected, the deposition of hydroxyapatite-like minerals only occurred in presence of osteogenic factors for ASCs-homotypic CS. Such results were evidenced in EDS (**Figure S9**) and OsteoImage^{TM} Assay (**Figure S10** and **Figure S11**). Similar to osteopontin staining and ALP activity, an enhanced mineralization was obtained for the heterotypic CSs in both basal and osteogenic media, which again anticipated the synergetic effect between the two cell phenotypes and consequently the osteogenic differentiation of ASCs in the presence of MC3T3-E1.

3.3.4. Cytokines Detection

The presence of the late osteogenic markers osteopontin and osteocalcin were exhibited in the heterotypic CS after 21 days even in the absence of osteogenic factors (**Figure 5D** and **E**). ASCs-homotypic CSs did not secrete cytokines without osteogenic supplementation. For both culturing conditions, the heterotypic CSs presented higher expression of such osteogenic markers than the MC3T3-homotypic CS, suggesting an osteogenic role of MC3T3-E1 over ASCs, inducing their osteogenic differentiation. Furthermore, the secretion of human bone morphogenic protein-2 (BMP-2) and vascular endothelium growth factor (VEGF) was also determined after 21 days (**Figure 5F** and **G**). These two cytokines synergistically interact to promote the angiogenesis while guarantying the proper bone formation.

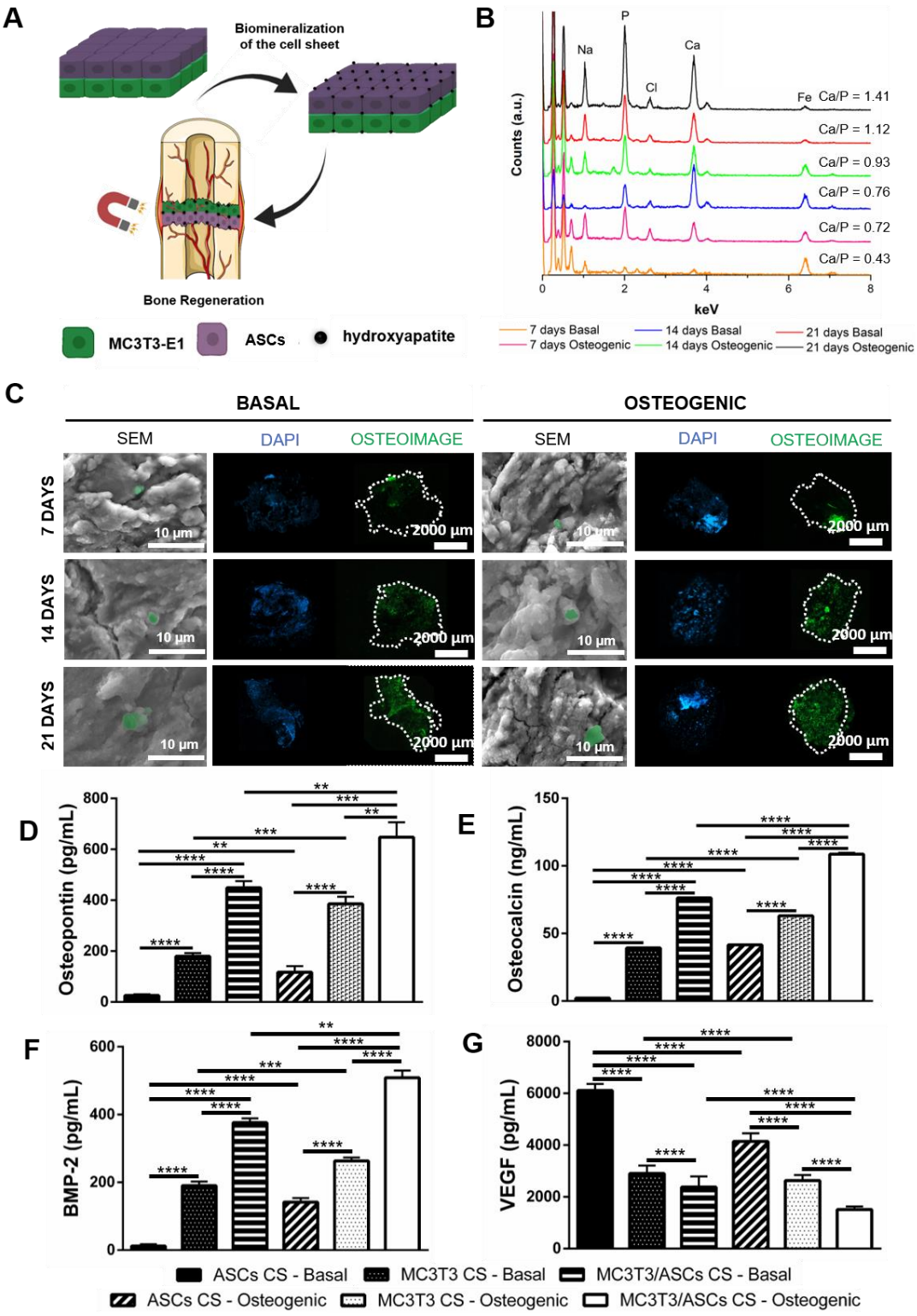

Figure 5. *In vitro* mineralization of the fabricated 3D heterotypic CSs in both culturing conditions. **A.** Schematic representation of the potential applications of the calcified tissues; **B.** Analysis of the mineral deposition within the CS by Energy dispersive X-ray spectroscopy (EDS); **C.** The deposition of the hydroxyapatite portion of bone-like nodules was also accessed through OsteoImage^{TM} fluorescence assay: cell nucleus - DAPI (blue) and hydroxyapatite (green). Calcium deposits are also represented in SEM micrographs (in green) - in the right panel; Quantification of osteopontin (D) and osteocalcin (E) BMP-2 (F) and VEGF (G) expressions by ELISA. $p < 0.05$: *$p < 0.05$; **$p < 0.01$; ***$p < 0.001$; ****$p < 0.0001$.

In this work, heterotypic CSs and MC3T3-homotypic CS presented an enhanced expression of BMP-2, even in basal conditions. In contrast, the higher level of VEGF was obtained in ASCs-homotypic CS cultured in basal conditions. In fact, ASCs stimulate blood vessels growth by the secretion of growth factors like VEGF. The down-regulation of VEGF level combined with higher values of BMP-2 indicated the osteogenic differentiation of ASCs, that once differentiated lose their ability to enhance the angiogenesis by decreasing the level of VEGF .[10,33] Altogether, our results demonstrated decreased levels of VEGF with an enhanced expression of BMP-2, therefore confirming that osteogenic differentiation had occurred for both ASCs-homotypic CS in osteogenic conditions and heterotypic CSs (both culturing conditions).

3.3.5. Histological cross-sections

The mineralization of the proposed heterotypic CS was also demonstrated by the presence of the late-stage differentiation marker osteocalcin in the histological sections of the CSs. Similar to previous results, an enhanced deposition of osteocalcin was verified for both culture conditions in the heterotypic CS. Moreover, the formation of bone-like tissue was confirmed through the presence of lamin A, a protein of the nuclear envelope that is required for normal bone turnover,[34] and by the expression of CD44, an transmembrane glycoprotein involved in bone formation.[35,36] Again, the presence of such markers was verified after 21 days in both culturing conditions (**Figure 6**).

To corroborate the enhanced mineralization of the proposed heterotypic CS, the presence of calcium deposits was also accessed in the cross-sections of the CS through a Von Kossa staining. **Figure 7** reveals the deposition of calcium minerals within the *de novo* matrix formation after 21 days in both culturing conditions.

Moreover, the deposition of ECM within the heterotypic CS was accessed by Trichrome Masson, fibronectin and collagen IV stainings (**Figure 6, 7**). Results show that the proposed

tissue-like constructs are composed by a dense ECM with a collagen enriched matrix in both culturing conditions (**Figure 7** and **Figure S12**).

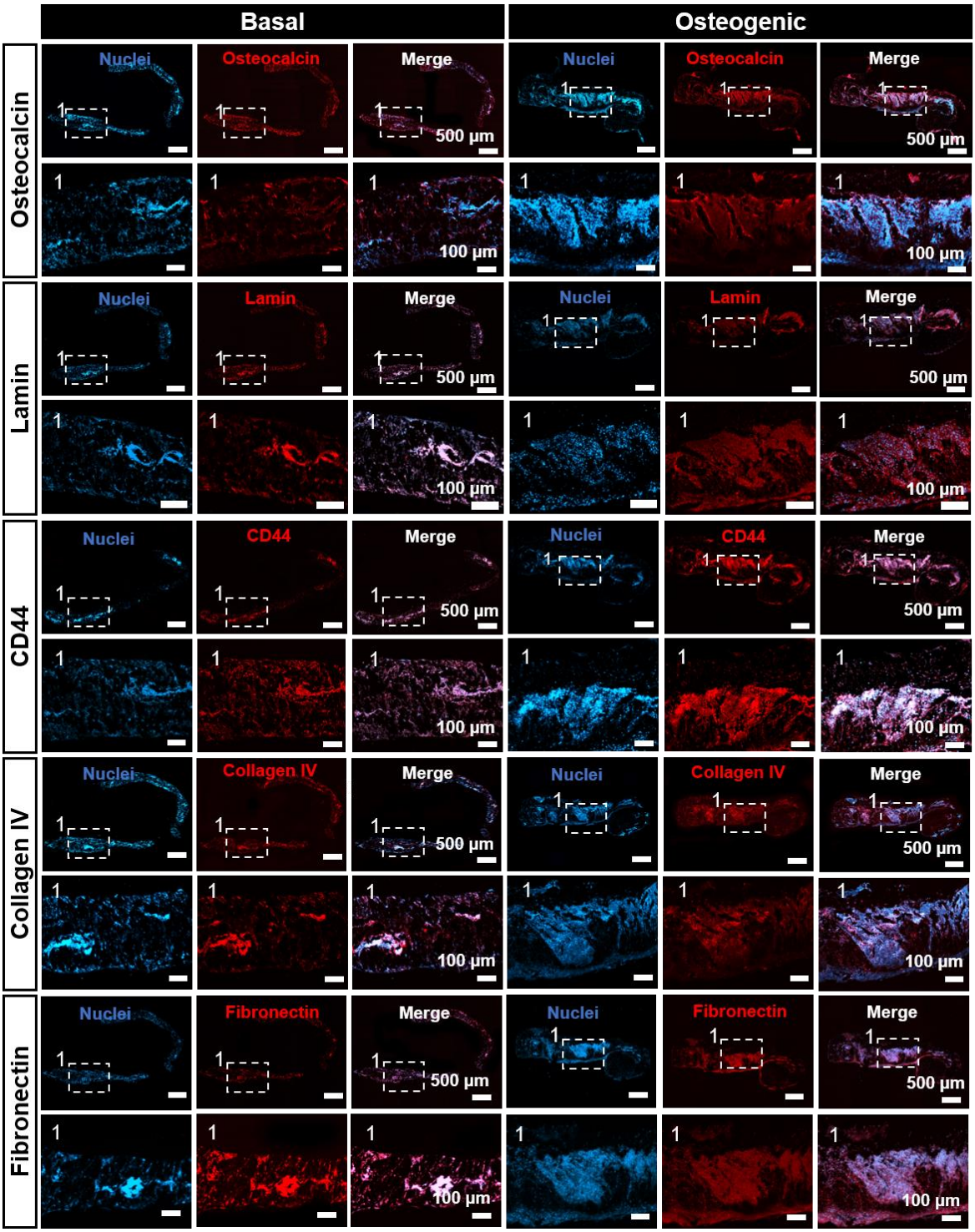

Figure 6. Immunostaining of paraffin-embedded heterotypic CS after 21 days in both culturing conditions: osteocalcin, lamin A, CD44, collagen IV and fibronectin (red) and DAPI (in blue) stains all nuclei.

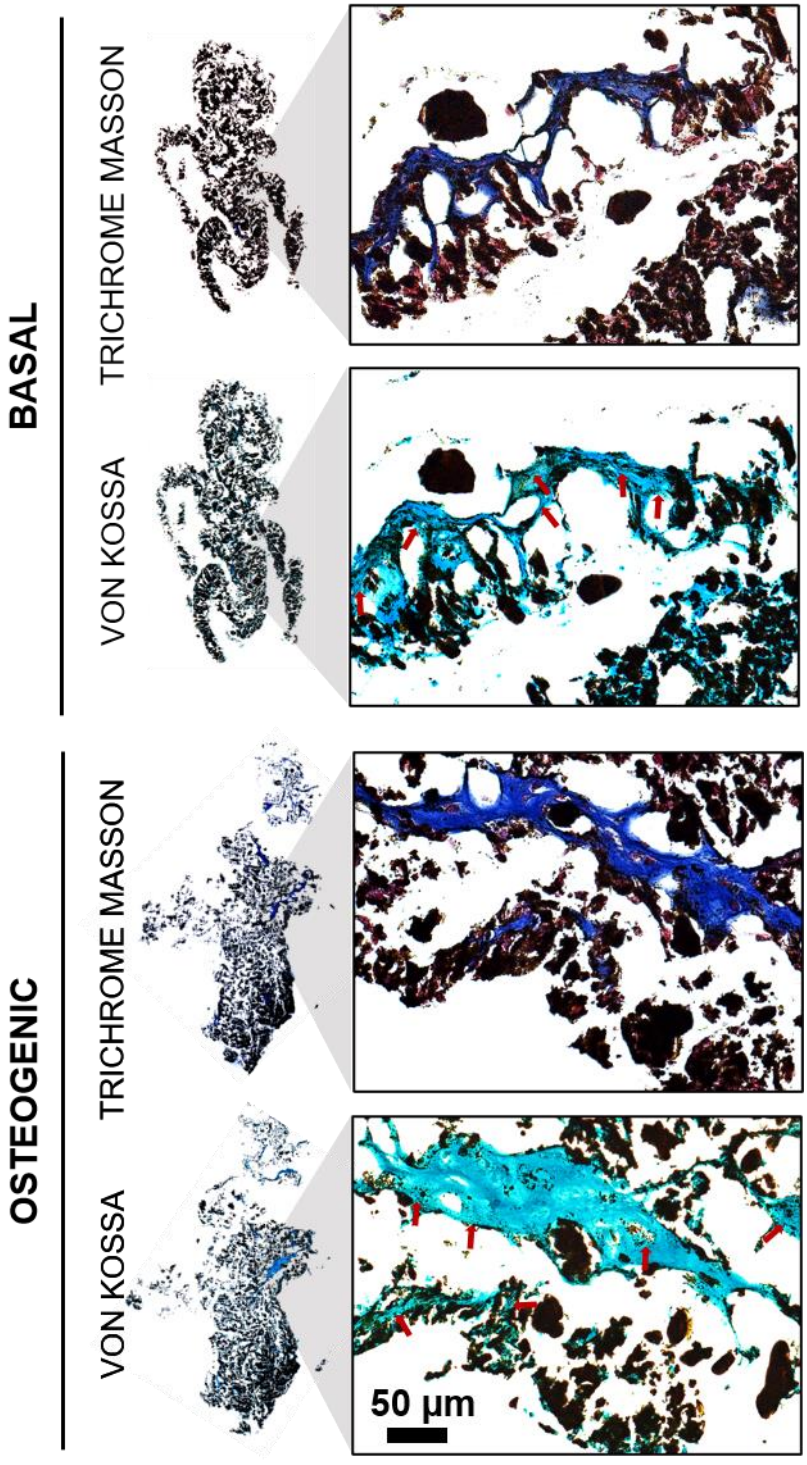

Figure 7. Histological sections of heterotypic CS cultured under basal (**A**) and osteogenic media (**B**) after 21 days. Trichrome Masson staining displays the collagenous connective tissue fibers and Von Kossa staining corroborates the mineralization of the heterotypic CS (calcium deposits are identified with red arrows).

4. Discussion

CS technology enables the fabrication of an entirely natural neo-tissue assembled by cells with mature ECM.[29] Nevertheless, one of the major shortcomings in the fabrication of 3D cell-like tissue from CSs is their poor mechanical properties that not only makes handling difficult, but also could compromises the proper function of tissue-like constructs.[15] Moreover, CSs tend to contract when removed from culture surfaces resulting in reduced graft sizes. Such limitations can be overcome through the construction of thicker tissues, with adequate morphologies and dimensions to fit several defects, guarantying the natural architecture of the living tissues.[37]

Within tissues and organs, cell-cell interactions are essential to maintain normal physiological conditions, playing a fundamental role in the regulation of the proliferation and differentiation of tissues.[38] In particular, homotypic and heterotypic cell-cell interactions are believed to be important in the activation of the cellular functions and in the development of more rigid and strong structures.[17] Current methodologies to produced stratified and heterotypic CSs comprise the use of the well-described thermo-responsive surfaces often associated with extra apparatus like CS layering manipulator or even automatic devices,[39,40] which requires user-knowledge, a clean room and the cost for apparatus fabrication. Moreover, such methodologies are also correlated with several constrains such as high cost, alteration of cell physiology and restriction in tissue replacement.[15,41] To overcome such limitations, Mag-TE have prompted the combination of magnetite nanoparticles and magnetic force in TE applications.[18] Cells are previously labelled with magnetic nanoparticles and then, external magnetic force promote cell-cell interactions. Magnetic cells are herein employed as building blocks for the construction of 3D tissues without requiring further artificial scaffolds. In addition, magnetic resonance imaging has been also exploring these magnetic cells as a promising candidates to assess the implanted cells and tissues, in an easier, rapid and non-invasive manner.[42,43] Despite of the

physical modifications and biodegradation of MNPs along the time, it is reported that living organisms present an excellent tolerance profile for smaller spherical iron oxide nanoparticles, coordinating specific mechanisms that retard the release of free cytotoxic iron ions, until being released in a safe form.[44] Our group has been exploring the development of hierarchical 3D tissues by Mag-TE in a simple, one-pot and time-saving manner.[10] Nevertheless, the problematic associated with high complexity of living tissues and poor mechanical properties of CSs prevails and restricts their use in the creation 3D-like tissues.[37] Based on this knowledge, we herein proposed the fabrication of mechanically strong and complex-shaped magnetic CSs with an ordered and stratified conformation able to mimic the native structure of tissues. Although we hypothesized that such organization could be used for bone TE purposes, we anticipate that the methodology herein proposed could be further used for the creation of wide range of 3D-tissues with diverse morphologies, thus demonstrating the ability of this technology in the fabrication of different CSs shapes able to fit specific tissue defects.

After confirming the successful construction of homotypic CSs composed by MC3T3-E1, we herein report the construction of robust homotypic CSs with enhanced mechanical properties using the MC3T3-E1 cell line. To the best of our knowledge, this is the first time that the mechanical behavior of cell-based constructs was accessed. In fact, an Young's Modulus of 22 ± 5 kPa was obtained for this type of CS, attaining similar values to the ones reported in the literature for soft tissues namely cornea, breast tissue, muscle and skin.[38,45] Moreover, the Young's modulus of our engineered tissue is analogous to the cartilaginous tissue model, ranging from 9 to 42 kPa.[46] Regarding the elongation rate, we herein obtained the value of 55 ± 6 % that is also similar to those find in bone-guided membranes.[47,48] Such flexible behavior represents an advantage in CS engineering by providing an easier handling of CSs that are normally damaged during the recovery process.[49] To explore the versatility of such methodology, we developed complex-shaped homotypic CSs with round, ring and concave shape exploring different types of substrates and magnet shapes. Such achievement testified the

advantage of Mag-TE in the construction of tissues able to fit different shapes of defects, thus expanding their application in the TE field. Additionally, the role of cell density in CS's thickness and robustness was also investigated along time (7, 14 and 21 days). As expected, we obtained more robust CSs with increased cell density. Literature reports that the lack of sufficient vascularization induces necrosis in bioengineered tissue thicker than 100–200 μm.[20] In this work, our constructs presented the maximum thickness of 70.5 μm without displaying risks of necrosis. Nevertheless, the thickness of the CS decreased along the time, which demonstrated more CS confine and thus suggested greater cell-cell interactions and CS stratification.[50] In 3D-like constructs, the establishment of heterogeneous cell culture systems is crucial to mimic tissues and organs. [51] By taking advantage of this knowledge, we hypothesized the possibility to create stratified heterotypic CSs by magnetically forcing both homotypic and heterotypic cell-cell interactions. For the purpose, magnetically labelled ASCs were seeded on top of a previously assembled (24 h before) monolayer of magnetically labelled MC3T3-E1, creating a CS with a double layer conformation. To attest the interaction between the two cell phenotypes within the CS, we evaluated the ability of MC3T3-E1 inducing osteogenic differentiation over ASCs, even in the absence of osteogenic supplements. Firstly, MC3T3-E1 and ASCs-homotypic CSs were successfully engineered (**Figure 1**) and used as controls. Then, the heterotypic CS with a double layer conformation was developed, as demonstrated by confocal microscopy (**Figure 3A**). After confirming their structural conformation by SEM, the cell-cell interactions within the heterotypic CS were also confirmed through a vinculin red-staining (**Figure 3C**). Later, the synergetic interaction between MC3T3-E1 and ASCs was confirmed through the osteogenic differentiation of the CSs. MC3T3-E1, as pre-osteoblastic cell linage, has been widely explored as model for *in vitro* osteoblast differentiation. In fact, MC3T3-E1 present similar behavior to primary osteoblasts and are already anticipated to exhibit osteogenic markers.[52] Previous works showed that osteoblasts have a great ability to modulate the osteogenic differentiation of stromal cells without requiring

any osteogenic supplementation.[52–54] However, to the best of our knowledge such behavior was never tested in layered scaffold-free structures.

The stemness of ASCs-homotypic CS, corroborated by the absence of osteogenic markers over time, and the increased concentration of osteogenic markers in the heterotypic CS suggested a positive effect of MC3T3-E1 over ASCs osteogenic differentiation. The stagnation on the metabolic activity together with increased ALP activity (normalized by area) suggested osteogenic differentiation of the heterotypic CS and MC3T3-homotypic CS in both culturing conditions. In contrast, the osteogenic differentiation of the ASCs-homotypic CS only occurred in the presence of osteogenic differentiation factors. Such results corroborated the hypothesis that MC3T3-E1 induced ASCs differentiation in such layered structures. The combination of ASCs CS with MC3T3-E1 CS showed an increment on ALP activity, even with basal culture medium. When compared to heterotypic CS, the homotypic CSs presented a decreased metabolic activity after 21 days, which suggested that the stratification of tissues could promote greater CS's nutrition and consequently cell survival and viability.[55]

Native bone tissue presents an hierarchical organization that comprises both non-mineralized organic component (predominantly Collagen type I) and a mineralized inorganic component composed by apatite minerals.[55] By taking advantage of this expertise, we explored the presence of such indicators in the proposed CSs to demonstrate the potential of this methodology in the creation of mineralized 3D-like *in vitro* tissues.[56] Thick and collagen-enriched matrices were verified in the heterotypic CSs cultured with or without osteogenic differentiation factors. These non-collagenous proteins, including collagen I, ostepontin and osteocalcin, are involved in bone matrix organization and in the intracellular signaling during the osteogenic differentiation, including in the recruitment of osteoblasts to the injured bone and regulation of bone structure and morphology.[57,58] According to **Figure 4** and **Figure 5D**, osteopontin started to be expressed at day 7, especially when CSs were cultured with osteogenic differentiating factors. Nevertheless, similar results were obtained for the

heterotypic CSs in both culturing conditions after 21 days. A similar tendency was also observed for the secretion of osteocalcin. Moreover, the heterotypic CSs presented higher expression of such osteogenic markers than the MC3T3-E1 homotypic CS, thus suggesting the osteogenic role of the MC3T3-E1 over ASCs. As anticipated, ASCs-homotypic CS only expressed such cytokines under osteogenic supplementation. Such results corroborated the ALP trends above mentioned. Additionally, we also evaluated the mineral component of bone-like tissue that normally comprises a crystalline complex of calcium and phosphate commonly denominated hydroxyapatite.[59] The results of OsteoImage^{TM} demonstrated similar deposition of hydroxyapatite in basal and osteogenic culturing conditions after 21 days, thus suggesting the synergetic interaction between MC3T3-E1 and ASCs within the heterotypic CS. To corroborate these results, the chemical composition of such minerals was also assessed. Once again, analogous Ca/P ratios were obtained after 21 days with both culturing conditions. In fact, the Ca/P ratio was similar to the one found in the apatite minerals in bone matrix, thus suggesting the tendency of the heterotypic CS in simulating the natural structure of bone.[60] After 21 days, the formation of bone-like tissue was also validated through the expression of fibronectin, lamin A, CD44 in both culturing conditions, essential for proper bone formation.[34–36] Moreover, the fibronectin and collagen IV are crucial to the matrix assembly and formation of sheet-like ECM of multicellular tissues, respectively.[61] Such essential ECM proteins were found in the heterotypic CSs developed for both culturing conditions. Additionally, ASCs and osteoblasts are known to be involved in blood vessels formation by secreting pro-angiogenic factors, such as VEGF, combining osteogenesis and vascularization during bone development and growth.[62,63] In this sense, VEGF and BMP-2 have been widely explored in TE to synergically incite angiogenesis and bone formation.[10,64] As anticipated, the heterotypic CSs secreted the highest amount of BMP-2 and more pronounced effect was noticed upon the supplementation with osteogenic differentiating factors. Such results corroborated our hypothesis that the co-culture of ASCs and MC3T3-E1 induced an enhanced

release of BMP-2. Moreover, the synergic behavior between VEGF and BMP-2 was also visualized in the developed CSs. Heterotypic CSs and MC3T3-homotypic CS demonstrated an increased osteogenic differentiation after 21 days, presenting low expression of VEGF and consequently, a diminished capacity to induce angiogenesis. Nevertheless, thick and high-dense CSs without adequate vascularization are reported to induce necrosis in tissues.[65,66] To overcome this limitation, the group proved that co-culture with endothelial cells could improve the angiogenic potential of the 3D construct, showing outstanding results in the migration and integration of the CS within the host.[10]

By providing magnetic cells as building blocks, we herein proposed the fabrication of mechanically strong and complex-shaped 3D-like tissues using Mag-TE in a simple, versatile, cost-effective and time-saving fashion. By simply adjusting the shapes of magnet and substrates we could obtain tissue-like constructs to be employed in diverse tissue defects, adapting the cell phenotypes of the CS to be fabricated. Regarding the current biofabrication strategies including the highly-explored 3D bioprinting, the strategy herein proposed does not require sophisticated apparatus or user-knowledge, which can prompt the fabrication of such tissue-like constructs in a large scale, overcoming the challenges of the remote control strategies in TE. 3D bioprinting is still not only facing technical challenges in terms of high-resolution cell deposition, controlled cell distributions and vascularization within complex 3D tissues but also require sophisticated apparatus, increasing the cost of the process and the need of user-knowledge.[67] As demonstrated by the group, the vascularization of the constructs is crucial to fabricate cell-dense tissues for supplying oxygen and nutrients while removing metabolic wastes.[10] According to previous works, this magnetic-based strategy showed the ability to engineer pre-vascularized constructs that were also able to migrate and integrate the host vasculature, overcoming the main issues of 3D bioprinting technique. Additionally, the capability to sequentially accommodate layers of different cells can be useful for the development of complex tissues using bottom-up TE strategies.[68]

By taking advantage of this expertise, the next steps of tissue manufacturing aim to recapitulate the geometry, complexity and architecture of human tissues while guarantying the survival of the 3D tissues and easier interaction with host tissue. An idyllic prospective of Mag-TE would encompass the fabrication of a total scaffold- and biomaterial-free tissue constructs, without internalization of MNPs within cells environment.

5. Conclusion

Current strategies for tissue manufacturing fail to recapitulate the geometry, complexity, strength and longevity of human tissues. Mag-TE has been implied in the production of more complex tissues that are not easily achieved by conventional TE methodologies. Herein, we anticipated that Mag-TE could enable the fabrication of versatile and robust 3D tissues with a biomimetic architecture based on cell phenotype and shapes of the magnet and substrate. Therefore, we proposed the construction of complex-shaped 3D-like tissues (CSs) in a simple, one-pot, versatile, cost-effective and time-saving strategy that could scale-up fabrication of 3D tissues. For the purpose, magnetic cells were used as building blocks and mechanical behavior of CSs was for the first time accessed. Moreover, we also evaluated the influence of cell density and time in the thickness of CSs, a crucial feature in the development of strong cellular constructs. As a proof-of-concept, we developed more complex and hierarchical 3D tissues using pre-osteoblast MC3T3-E1 cell line and ASCs in a double CS conformation. The ability of this construct for bone regeneration purposes was revealed even in the absence of osteogenic differentiation factors, attesting for the first time the role of the pre-osteoblast cell linage in stromal cells in such kind of living materials. Although this work is intended for bone TE, we anticipate that this methodology could be further extended for a plethora of organized tissues, opening new avenues for the fabrication of 3D constructs that better mimics the complex environmental of native tissues with potential applications in the production of *in vitro* disease models or implantable structures for tissue/organ repair and regeneration.

Acknowledgements

This work was developed within the scope of the project CICECO-Aveiro Institute of Materials, UIDB/50011/2020 & UIDP/50011/2020, financed by national funds through the FCT/MEC and when appropriate co-financed by FEDER under the PT2020 Partnership Agreement and PROMENADE (Ref. PTDC/BTM-MAT/29830/2017). This work was also sponsored by the project ATLAS (ref.ERC-2014-ADG-669858) and through the doctoral grant SFRH/BD/141523/2018 (Lúcia F. Santos).

References

[1] E.S. Place, J.H. George, C.K. Williams, M.M. Stevens, Synthetic polymer scaffolds for tissue engineering, Chem. Soc. Rev. 38 (2009) 1139–1151. https://doi.org/10.1039/b811392k.

[2] G. Chan, D.J. Mooney, New materials for tissue engineering: towards greater control over the biological response, Trends Biotechnol. 26 (2008) 382–392. https://doi.org/10.1016/j.tibtech.2008.03.011.

[3] X. Liu, P.X. Ma, Polymeric scaffolds for bone tissue engineering, Ann. Biomed. Eng. 32 (2004) 477–486. https://doi.org/10.1023/B:ABME.0000017544.36001.8e.

[4] F.J. O'Brien, Biomaterials & scaffolds for tissue engineering, Mater. Today. 14 (2011) 88–95. https://doi.org/10.1016/S1369-7021(11)70058-X.

[5] F.M. Chen, X. Liu, Advancing biomaterials of human origin for tissue engineering, Prog. Polym. Sci. 53 (2016) 86–168. https://doi.org/10.1016/j.progpolymsci.2015.02.004.

[6] A. Ovsianikov, A. Khademhosseini, V. Mironov, The Synergy of Scaffold-Based and Scaffold-Free Tissue Engineering Strategies, Trends Biotechnol. 36 (2018) 348–357. https://doi.org/10.1016/j.tibtech.2018.01.005.

[7] A. Atala, F. Kurtis Kasper, A.G. Mikos, Engineering complex tissues, Sci. Transl. Med. 4 (2012) 1–12. https://doi.org/10.1126/scitranslmed.3004890.

[8] A. Shahin-Shamsabadi, P.R. Selvaganapathy, Tissue-in-a-Tube: three-dimensional in vitro tissue constructs with integrated multimodal environmental stimulation, Mater. Today Bio. 7 (2020) 100070. https://doi.org/10.1016/j.mtbio.2020.100070.

[9] C. Norotte, F.S. Marga, L.E. Niklason, G. Forgacs, Scaffold-free vascular tissue engineering using bioprinting, Biomaterials. 30 (2009) 5910–5917. https://doi.org/10.1016/j.biomaterials.2009.06.034.

[10] A.S. Silva, L.F. Santos, M.C. Mendes, J.F. Mano, Multi-layer pre-vascularized magnetic cell sheets for bone regeneration, Biomaterials. 231 (2020) 119664. https://doi.org/10.1016/j.biomaterials.2019.119664.

[11] J. Yang, M. Yamato, C. Kohno, A. Nishimoto, H. Sekine, F. Fukai, T. Okano, Cell sheet engineering: Recreating tissues without biodegradable scaffolds, Biomaterials. 26 (2005) 6415–6422. https://doi.org/10.1016/J.BIOMATERIALS.2005.04.061.

[12] M. Yamato, T. Okano, Cell sheet engineering, Mater. Today. 7 (2004) 42–47. https://doi.org/10.1016/S1369-7021(04)00234-2.

[13] J. Yang, M. Yamato, T. Shimizu, H. Sekine, K. Ohashi, M. Kanzaki, T. Ohki, K. Nishida, T. Okano, Reconstruction of functional tissues with cell sheet engineering,

Biomaterials. 28 (2007) 5033–5043. https://doi.org/10.1016/j.biomaterials.2007.07.052.
[14] T. Owaki, T. Shimizu, M. Yamato, T. Okano, Cell sheet engineering for regenerative medicine: Current challenges and strategies, Biotechnol. J. 9 (2014) 904–914. https://doi.org/10.1002/biot.201300432.
[15] I.Y. Kim, R. Iwatsuki, K. Kikuta, Y. Morita, T. Miyazaki, C. Ohtsuki, Thermoreversible behavior of κ-carrageenan and its apatite-forming ability in simulated body fluid, Mater. Sci. Eng. C. 31 (2011) 1472–1476. https://doi.org/10.1016/J.MSEC.2011.05.015.
[16] A. Ito, Y. Takizawa, H. Honda, K. Hata, H. Kagami, M. Ueda, T. Kobayashi, Construction and Harvest of Multilayered Keratinocyte Sheets Using Magnetite Nanoparticles and Magnetic Force, Tissue Eng. 10 (2004) 873–880.
[17] E. Castro, J.F. Mano, Magnetic Force-Based Tissue Engineering and Regenerative Medicine, J. Biomed. Nanotechnol. 9 (2013) 1129–1136. https://doi.org/10.1166/jbn.2013.1635.
[18] A. Ito, Y. Takizawa, H. Honda, K. Hata, H. Kagami, M. Ueda, T. Kobayashi, Tissue Engineering Using Magnetite Nanoparticles and Magnetic Force: Heterotypic Layers of Cocultured Hepatocytes and Endothelial Cells, Tissue Eng. 10 (2004) 833–840. https://doi.org/10.1089/1076327041348301.
[19] J. Dobson, Remote control of cellular behaviour with magnetic nanoparticles, Nat. Nanotechnol. 3 (2008) 139–143. https://doi.org/10.1038/nnano.2008.39.
[20] N. Asakawa, T. Shimizu, Y. Tsuda, S. Sekiya, T. Sasagawa, M. Yamato, F. Fukai, T. Okano, Pre-vascularization of in vitro three-dimensional tissues created by cell sheet engineering, Biomaterials. 31 (2010) 3903–3909. https://doi.org/10.1016/j.biomaterials.2010.01.105.
[21] H. Akiyama, A. Ito, Y. Kawabe, M. Kamihira, Biomaterials Genetically engineered angiogenic cell sheets using magnetic force-based gene delivery and tissue fabrication techniques, Biomaterials. 31 (2010) 1251–1259. https://doi.org/10.1016/j.biomaterials.2009.11.017.
[22] T. Kito, R. Shibata, M. Ishii, H. Suzuki, T. Himeno, Y. Kataoka, Y. Yamamura, T. Yamamoto, N. Nishio, S. Ito, Y. Numaguchi, T. Tanigawa, J.K. Yamashita, N. Ouchi, H. Honda, K. Isobe, T. Murohara, iPS cell sheets created by a novel magnetite tissue engineering method for reparative angiogenesis, Sci. Rep. 3 (2013) 1418. https://doi.org/10.1038/srep01418.
[23] A. Ito, H. Jitsunobu, Y. Kawabe, M. Kamihira, Construction of Heterotypic Cell Sheets by Magnetic Force-Based 3-D Coculture of HepG2 and NIH3T3 Cells, J. Biosci. Bioeng. 104 (2007) 371–378. https://doi.org/10.1263/JBB.104.371.
[24] T. Courtney, M.S. Sacks, J. Stankus, J. Guan, W.R. Wagner, Design and analysis of tissue engineering scaffolds that mimic soft tissue mechanical anisotropy, Biomaterials. 27 (2006) 3631–3638. https://doi.org/10.1016/j.biomaterials.2006.02.024.
[25] S. Gil, C.R. Correia, J.F. Mano, Magnetically Labeled Cells with Surface-Modified Fe_3O_4 Spherical and Rod-Shaped Magnetic Nanoparticles for Tissue Engineering Applications, Adv. Healthc. Mater. 4 (2015) 883–891. https://doi.org/10.1002/adhm.201400611.
[26] T. Kikuchi, T. Shimizu, M. Wada, M. Yamato, T. Okano, Automatic fabrication of 3-dimensional tissues using cell sheet manipulator technique, Biomaterials. 35 (2014) 2428–2435. https://doi.org/10.1016/j.biomaterials.2013.12.014.
[27] G.J. Atkins, D.M. Findlay, P.H. Anderson, H.A. Morris, Target Genes: Bone Proteins, Vitam. D. 23 (2011) 411–424. https://doi.org/10.1016/B978-0-12-381978-9.10023-X.
[28] T. Kaito, A. Myoui, K. Takaoka, N. Saito, M. Nishikawa, N. Tamai, H. Ohgushi, H. Yoshikawa, Potentiation of the activity of bone morphogenetic protein-2 in bone

regeneration by a PLA-PEG/hydroxyapatite composite, Biomaterials. 26 (2005) 73–79. https://doi.org/10.1016/j.biomaterials.2004.02.010.
[29] N. Matsuda, T. Shimizu, M. Yamato, T. Okano, Tissue Engineering Based on Cell Sheet Technology, Adv. Mater. 19 (2007) 3089–3099. https://doi.org/10.1002/adma.200701978.
[30] H. Zhou, J. Lee, Nanoscale hydroxyapatite particles for bone tissue engineering, Acta Biomater. 7 (2011) 2769–2781. https://doi.org/10.1016/j.actbio.2011.03.019.
[31] B.W. T, J.D. Pasteris, A mineralogical perspective on the apatite in bone, 25 (2005) 131–143. https://doi.org/10.1016/j.msec.2005.01.008.
[32] S. Raynaud, E. Champion, Calcium phosphate apatites with variable Ca / P atomic ratio II . Calcination and sintering, 23 (2002) 1073–1080.
[33] C.R. Correia, R.P. Pirraco, M.T. Cerqueira, A.P. Marques, R.L. Reis, J.F. Mano, Semipermeable Capsules Wrapping a Multifunctional and Self-regulated Co-culture Microenvironment for Osteogenic Differentiation, Sci. Rep. 6 (2016) 21883. https://doi.org/10.1038/srep21883.
[34] W. Li, L.S. Yeo, C. Vidal, T. McCorquodale, M. Herrmann, D. Fatkin, G. Duque, Decreased Bone Formation and Osteopenia in Lamin A/C-Deficient Mice, PLoS One. 6 (2011) e19313. https://doi.org/10.1371/journal.pone.0019313.
[35] R. Sackstein, J.S. Merzaban, D.W. Cain, N.M. Dagia, J.A. Spencer, C.P. Lin, R. Wohlgemuth, Ex vivo glycan engineering of CD44 programs human multipotent mesenchymal stromal cell trafficking to bone, Nat. Med. 14 (2008) 181–187. https://doi.org/10.1038/nm1703.
[36] T.J. de Vries, T. Schoenmaker, W. Beertsen, R. van der Neut, V. Everts, Effect of CD44 deficiency on in vitro and in vivo osteoclast formation, J. Cell. Biochem. 94 (2005) 954–966. https://doi.org/10.1002/jcb.20326.
[37] C.K. Griffith, C. Miller, R.C.A. Sainson, J.W. Calvert, N.L. Jeon, C.C.W. Hughes, S.C. George, Diffusion limits of an in vitro thick prevascularized tissue, Tissue Eng. 11 (2005) 257–266. https://doi.org/10.1089/ten.2005.11.257.
[38] J.F. Mano, R.A. Sousa, L.F. Boesel, N.M. Neves, R.L. Reis, Bioinert, biodegradable and injectable polymeric matrix composites for hard tissue replacement: State of the art and recent developments, Compos. Sci. Technol. 64 (2004) 789–817. https://doi.org/10.1016/j.compscitech.2003.09.001.
[39] N. Asakawa, T. Shimizu, Y. Tsuda, S. Sekiya, T. Sasagawa, M. Yamato, F. Fukai, T. Okano, Pre-vascularization of in vitro three-dimensional tissues created by cell sheet engineering, Biomaterials. 31 (2010) 3903–3909. https://doi.org/10.1016/j.biomaterials.2010.01.105.
[40] N. Yamada, T. Okano, H. Sakai, F. Karikusa, Y. Sawasaki, Y. Sakurai, Thermo-responsive polymeric surfaces; control of attachment and detachment of cultured cells, Die Makromol. Chemie, Rapid Commun. 11 (1990) 571–576. https://doi.org/10.1002/marc.1990.030111109.
[41] M. Nakayama, T. Okano, F.M. Winnik, Poly(N-isopropylacrylamide)-based Smart Surfaces for Cell Sheet Tissue Engineering, Mater. Matters. 5 (2010) 56.
[42] H. Xu, S.F. Othman, R.L. Magin, Monitoring Tissue Engineering Using Magnetic Resonance Imaging, J. Biosci. Bioeng. 106 (2008) 515–527. https://doi.org/10.1263/jbb.106.515.
[43] K.. J. Saldanha, S.L. Piper, K.M. Ainslie, H.T. Kim, S. Majumdar, Magnetic resonance imaging of iron oxide labelled stem cells: applications to tissue engineering based regeneration of the intervertebral disc, Eur. Cells Mater. 16 (2008) 17–25. https://doi.org/10.22203/eCM.v016a03.
[44] L. Lartigue, D. Alloyeau, J. Kolosnjaj-Tabi, Y. Javed, P. Guardia, A. Riedinger, C. Péchoux, T. Pellegrino, C. Wilhelm, F. Gazeau, Biodegradation of iron oxide

nanocubes: High-resolution in situ monitoring, ACS Nano. 7 (2013) 3939–3952. https://doi.org/10.1021/nn305719y.
[45] C.T. McKee, J.A. Last, P. Russell, C.J. Murphy, Indentation versus tensile measurements of young's modulus for soft biological tissues, Tissue Eng. - Part B Rev. 17 (2011) 155–164. https://doi.org/10.1089/ten.teb.2010.0520.
[46] S. Miyata, T. Numano, K. Homma, T. Tateishi, T. Ushida, Feasibility of noninvasive evaluation of biophysical properties of tissue-engineered cartilage by using quantitative MRI, J. Biomech. 40 (2007) 2990–2998. https://doi.org/10.1016/j.jbiomech.2007.02.002.
[47] C. Xianmiao, L. Yubao, Z. Yi, Z. Li, L. Jidong, W. Huanan, Properties and in vitro biological evaluation of nano-hydroxyapatite/chitosan membranes for bone guided regeneration, Mater. Sci. Eng. C. 29 (2009) 29–35. https://doi.org/10.1016/j.msec.2008.05.008.
[48] M.A. Basile, G.G. D'Ayala, M. Malinconico, P. Laurienzo, J. Coudane, B. Nottelet, F. Della Ragione, A. Oliva, Functionalized PCL/HA nanocomposites as microporous membranes for bone regeneration, Mater. Sci. Eng. C. 48 (2015) 457–468. https://doi.org/10.1016/j.msec.2014.12.019.
[49] A. Ito, K. Ino, T. Kobayashi, H. Honda, The effect of RGD peptide-conjugated magnetite cationic liposomes on cell growth and cell sheet harvesting, Biomaterials. 26 (2005) 6185–6193. https://doi.org/10.1016/J.BIOMATERIALS.2005.03.039.
[50] T.J. Klein, B.L. Schumacher, T.A. Schmidt, K.W. Li, M.S. Voegtline, K. Masuda, E.J.M.A. Thonar, R.L. Sah, Tissue engineering of stratified articular cartilage from chondrocyte subpopulations, Osteoarthr. Cartil. 11 (2003) 595–602. https://doi.org/10.1016/S1063-4584(03)00090-6.
[51] Y. Haraguchi, T. Shimizu, M. Yamato, T. Okano, Scaffold-free tissue engineering using cell sheet technology, RSC Adv. 2 (2012) 2184–2190. https://doi.org/10.1039/c2ra00704e.
[52] A. Birmingham, L.M. McNamara, Osteogenic differentiation of mesenchymal stem cells is regulated by osteocyte and osteoblast cells in a simplified bone niche, Eur. Cells Mater. 23 (2012) 13–27. www.ecmjournal.org (accessed November 28, 2019).
[53] A. Tevlek, S. Odabas, E. Çelik, H.M. Aydin, Preparation of MC3T3-E1 cell sheets through short-term osteogenic medium application, Artif. Cells, Nanomedicine, Biotechnol. 46 (2018) 1145–1153. https://doi.org/10.1080/21691401.2018.1481081.
[54] S. Nadine, S.G. Patrício, C.R. Correia, J.F. Mano, Dynamic microfactories co-encapsulating osteoblastic and adipose-derived stromal cells for the biofabrication of bone units, Biofabrication. 12 (2019) 015005. https://doi.org/10.1088/1758-5090/ab3e16.
[55] M.M. Stevens, Biomaterials for bone tissue engineering, Mater. Today. 11 (2008) 18–25. https://doi.org/10.1016/S1369-7021(08)70086-5.
[56] M.B. Keogh, F.J. O'Brien, J.S. Daly, A novel collagen scaffold supports human osteogenesis - Applications for bone tissue engineering, Cell Tissue Res. 340 (2010) 169–177. https://doi.org/10.1007/s00441-010-0939-y.
[57] Z. Lin, K.L. Solomon, X. Zhang, N.J. Pavlos, T. Abel, C. Willers, K. Dai, J. Xu, Q. Zheng, M. Zheng, In vitro evaluation of natural marine sponge collagen as a scaffold for bone tissue engineering, Int. J. Biol. Sci. 7 (2011) 968–977. https://doi.org/10.7150/ijbs.7.968.
[58] R. Marom, I. Shur, R. Solomon, D. Benayahu, Characterization of adhesion and differentiation markers of osteogenic marrow stromal cells, J. Cell. Physiol. 202 (2005) 41–48. https://doi.org/10.1002/jcp.20109.
[59] T.A. Grünewald, H. Rennhofer, B. Hesse, M. Burghammer, S.E. Stanzl-Tschegg, M. Cotte, J.F. Löffler, A.M. Weinberg, H.C. Lichtenegger, Magnesium from bioresorbable

implants: Distribution and impact on the nano- and mineral structure of bone, Biomaterials. 76 (2016) 250–260. https://doi.org/10.1016/j.biomaterials.2015.10.054.
[60] B. Wopenka, J.D. Pasteris, A mineralogical perspective on the apatite in bone, Mater. Sci. Eng. C. 25 (2005) 131–143. https://doi.org/10.1016/J.MSEC.2005.01.008.
[61] C. Werner, T. Pompe, K. Salchert, Modulating extracellular matrix at interfaces of polymeric materials, Adv. Polym. Sci. 203 (2006) 63–93. https://doi.org/10.1007/12_089.
[62] M.M.L. Deckers, R.L. van Bezooijen, G. van der Horst, J. Hoogendam, C. van der Bent, S.E. Papapoulos, C.W.G.M. Löwik, Bone Morphogenetic Proteins Stimulate Angiogenesis through Osteoblast-Derived Vascular Endothelial Growth Factor A, Endocrinology. 143 (2002) 1545–1553. https://doi.org/10.1210/endo.143.4.8719.
[63] F. Verseijden, H. Jahr, S.J. Posthumus-van Sluijs, T.L. Ten Hagen, S.E.R. Hovius, A.L.B. Seynhaeve, J.W. van Neck, G.J.V.M. van Osch, S.O.P. Hofer, Angiogenic Capacity of Human Adipose-Derived Stromal Cells During Adipogenic Differentiation: An *In Vitro* Study, Tissue Eng. Part A. 15 (2009) 445–452. https://doi.org/10.1089/ten.tea.2007.0429.
[64] X. Jiang, D.L. Kaplan, VEGF and BMP-2 promote stem cell homing, Eur. Cells Mater. 27 (2014) 1–12. https://doi.org/10.22203/eCM.v027a01.
[65] K. Moschouris, N. Firoozi, Y. Kang, The application of cell sheet engineering in the vascularization of tissue regeneration, Regen. Med. 11 (2016) 559–570. https://doi.org/10.2217/rme-2016-0059.
[66] Y. Naka, S. Kitano, S. Irie, M. Matsusaki, Wholly vascularized millimeter-sized engineered tissues by cell-sized microscaffolds, Mater. Today Bio. 6 (2020) 100054. https://doi.org/10.1016/j.mtbio.2020.100054.
[67] E.S. Bishop, S. Mostafa, M. Pakvasa, H.H. Luu, M.J. Lee, J.M. Wolf, G.A. Ameer, T.C. He, R.R. Reid, 3-D bioprinting technologies in tissue engineering and regenerative medicine: Current and future trends, Genes Dis. 4 (2017) 185–195. https://doi.org/10.1016/j.gendis.2017.10.002.
[68] V.M. Gaspar, P. Lavrador, J. Borges, M.B. Oliveira, J.F. Mano, Advanced Bottom-Up Engineering of Living Architectures, Adv. Mater. 6 (2019) 1903975. https://doi.org/10.1002/adma.201903975.

Supplementary material

Mechanically strong and complex-shaped magnetic 3D tissues for tissue engineering applications

Lúcia F. Santos, A. Sofia Silva, João F. Mano**

[1]CICECO-Aveiro Institute of Materials, Department of Chemistry, University of Aveiro Campus de Santiago, 3810-193 Aveiro, Portugal

Corresponding authors: sofiamsilva@ua.pt; jmano@ua.pt

Contents

Figure S12 - Percentage of osteocalcin, lamin, CD44, fibronectin and collagen IV in the representative histological cuts.

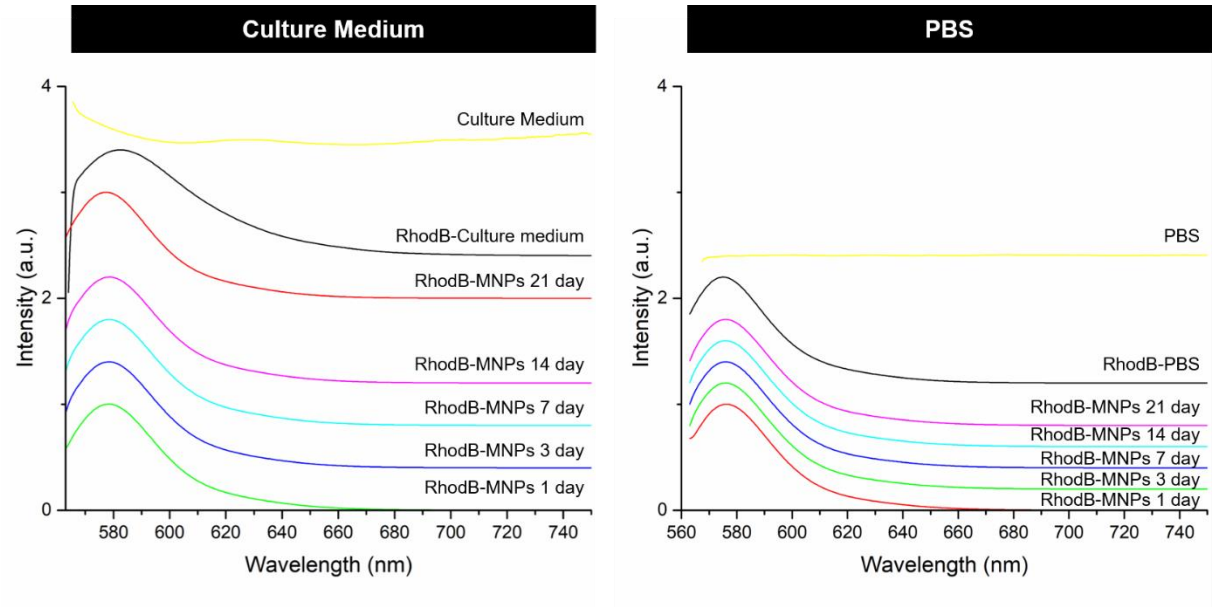

Figure S1. Stability of RhodB-MNPs incubated in dPBS and α-MEM culture medium during 21 days at 37°C.

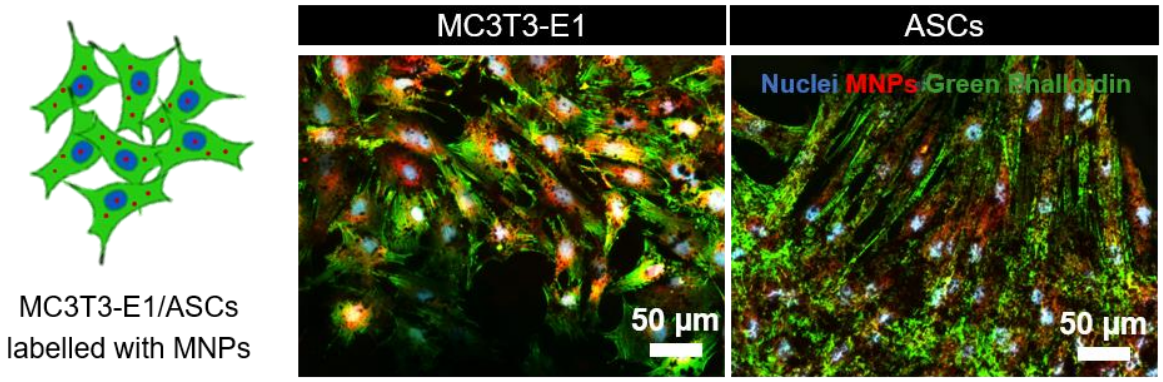

Figure S2. Cellular uptake of RhodB-MNPs in ASCs and MC3T3-E1: actin filaments of MC3T3-E1 and ASCs (green phalloidin), RhodB-MNPs (red) and cell nucleus - DAPI (blue).

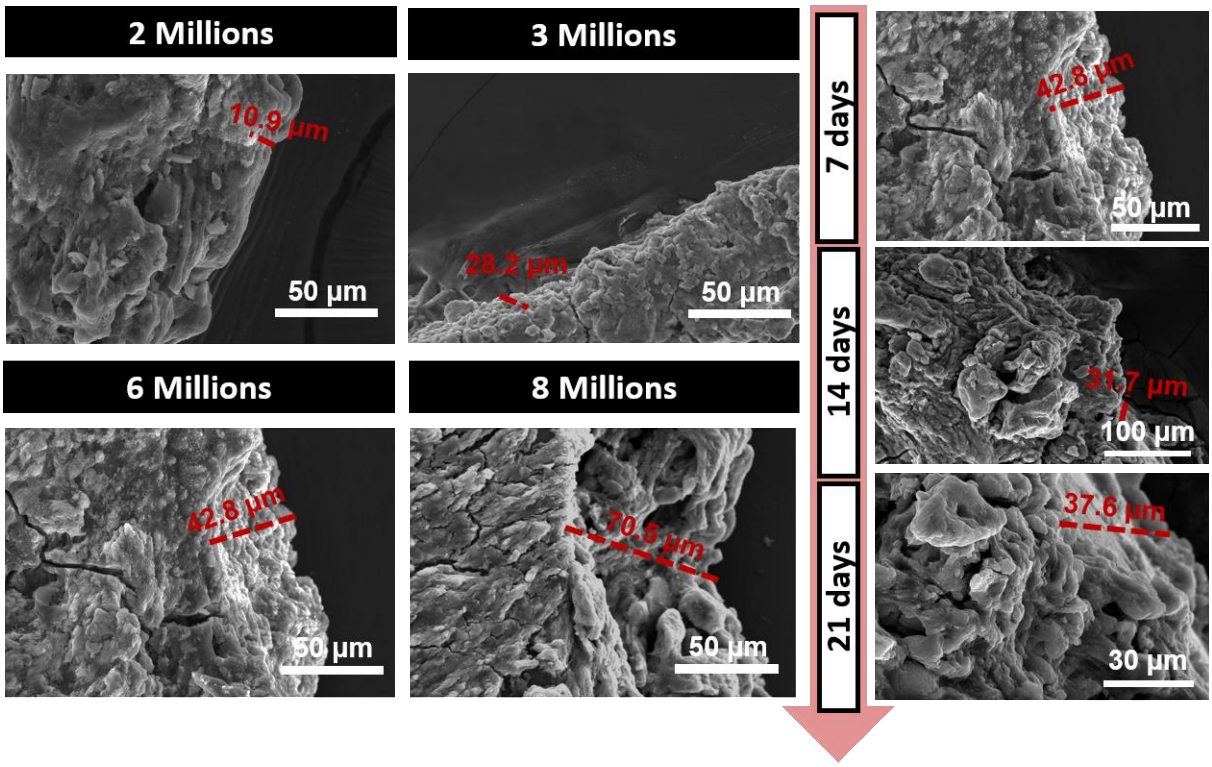

Figure S3. SEM micrographs of the developed MC3T3-homotypic CS with different cell density (namely 2, 3, 6 and 8 million cells) and along the time (at 7, 14 and 21 days).

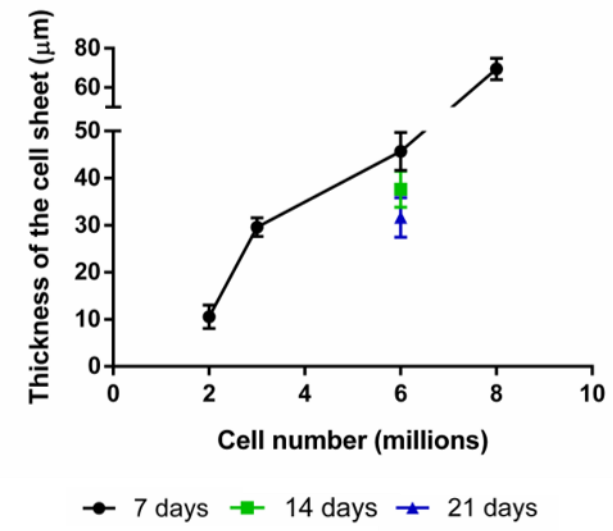

Figure S4. Graphical representation of the thickness of the CS along the time and varying the cell density.

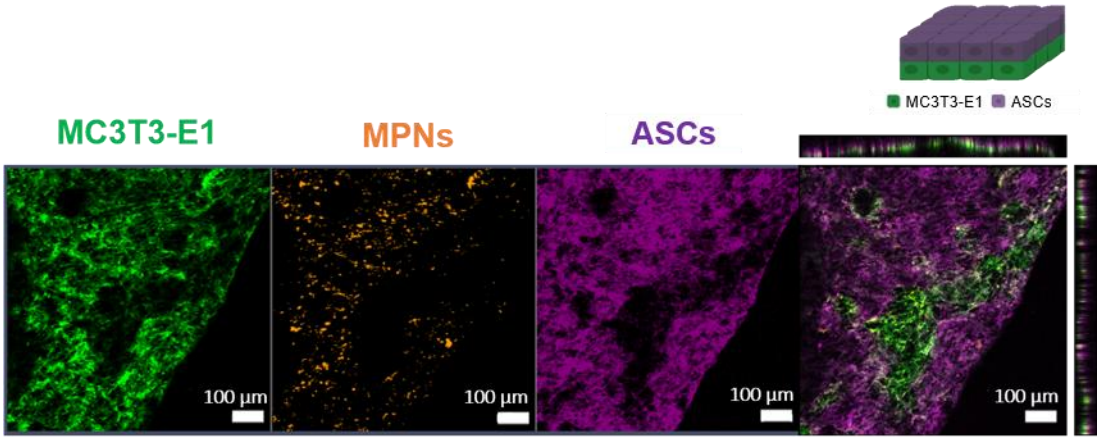

Figure S5. Confocal microscopy of the magnetically labelled CS composed by MC3T3-E1 (green) and ASCs (purple) in double sheet conformation.

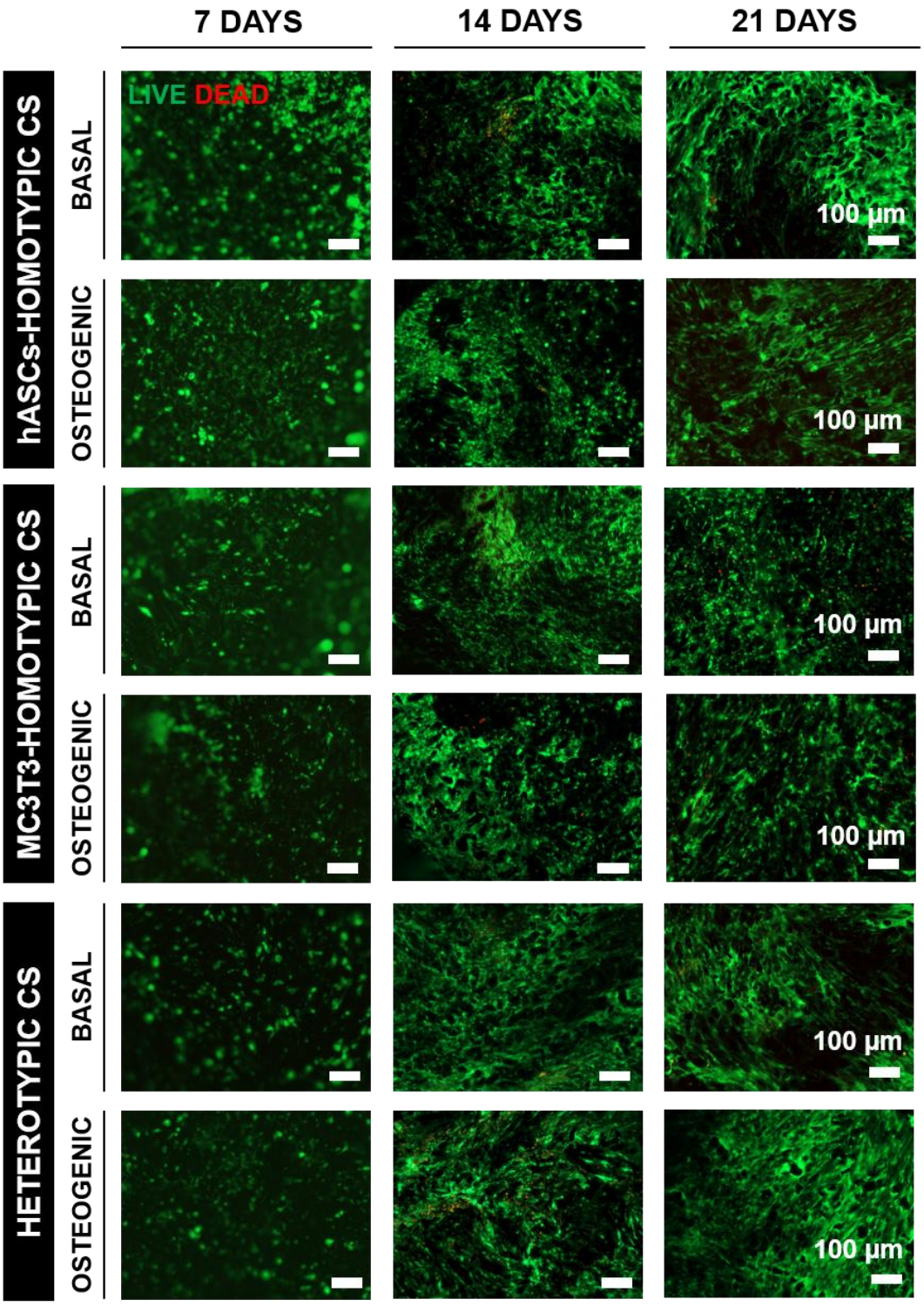

Figure S6*:* Live-dead fluorescence assay *of homotypic and heterotypic CSs after* 7, 14 and 21 of culture in basal and osteogenic *conditions.* Living cells were stained by calcein (green) and dead cells by propidium iodide (red).

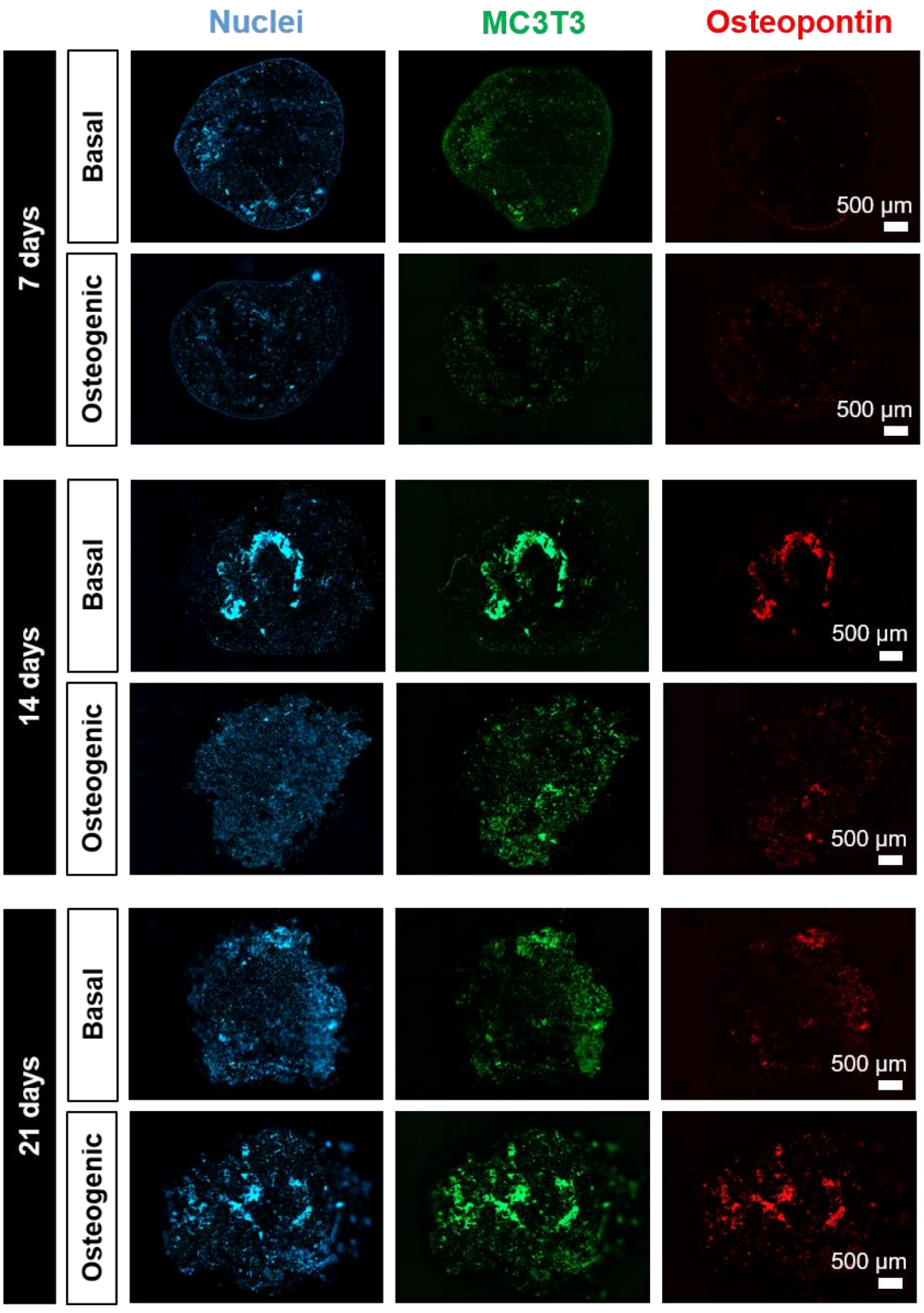

Figure S7. Immunofluorescence of MC3T3-homotypic CS after 7, 14 and 21 days in both culture conditions: MC3T3-E1 (green), osteopontin (red) and cell nucleus-DAPI (blue).

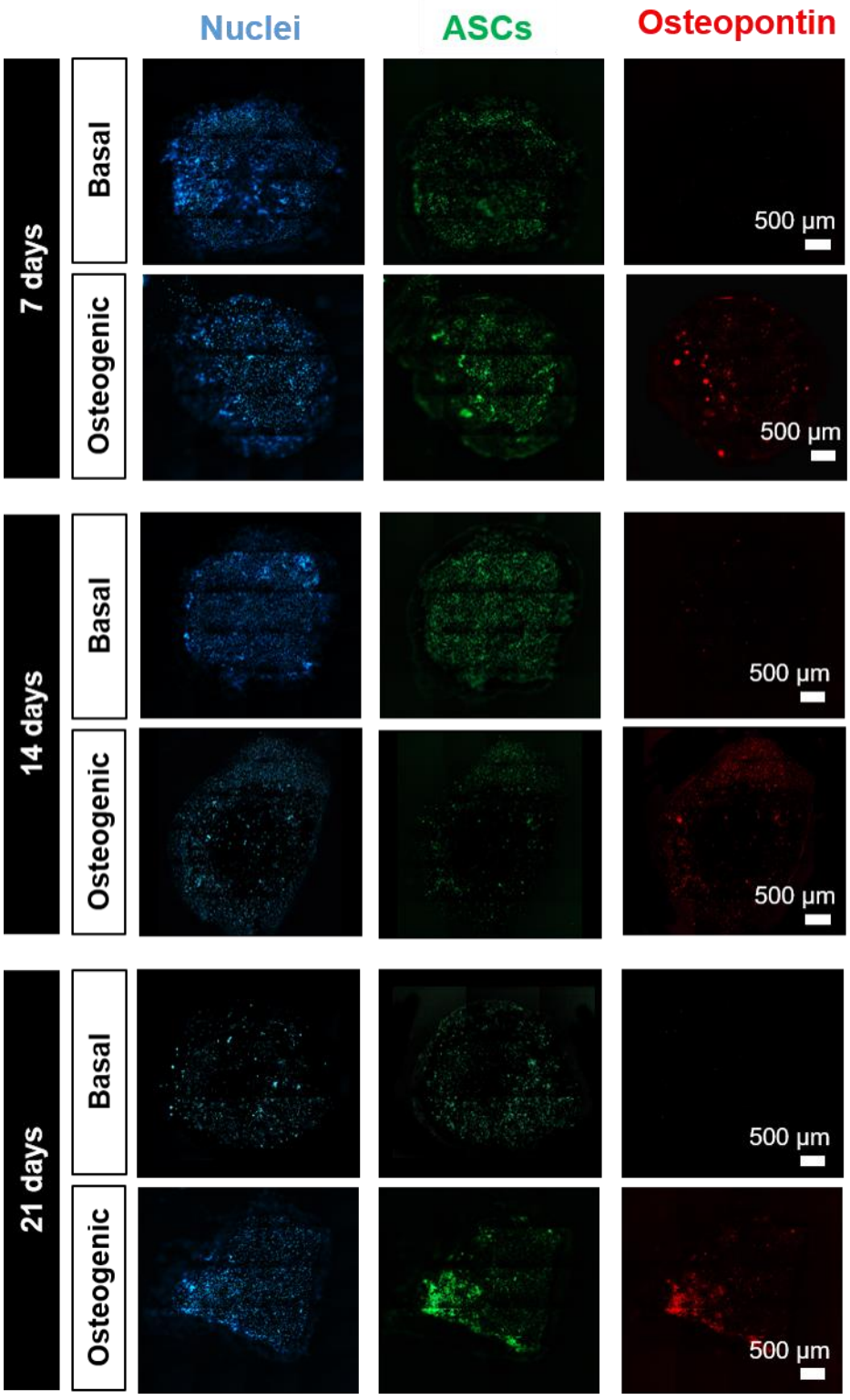

Figure S8. Immunofluorescence of ASCs-homotypic CS after 7, 14 and 21 days in both culture conditions: ASCs (green), osteopontin (red) and cell nucleus-DAPI (blue).

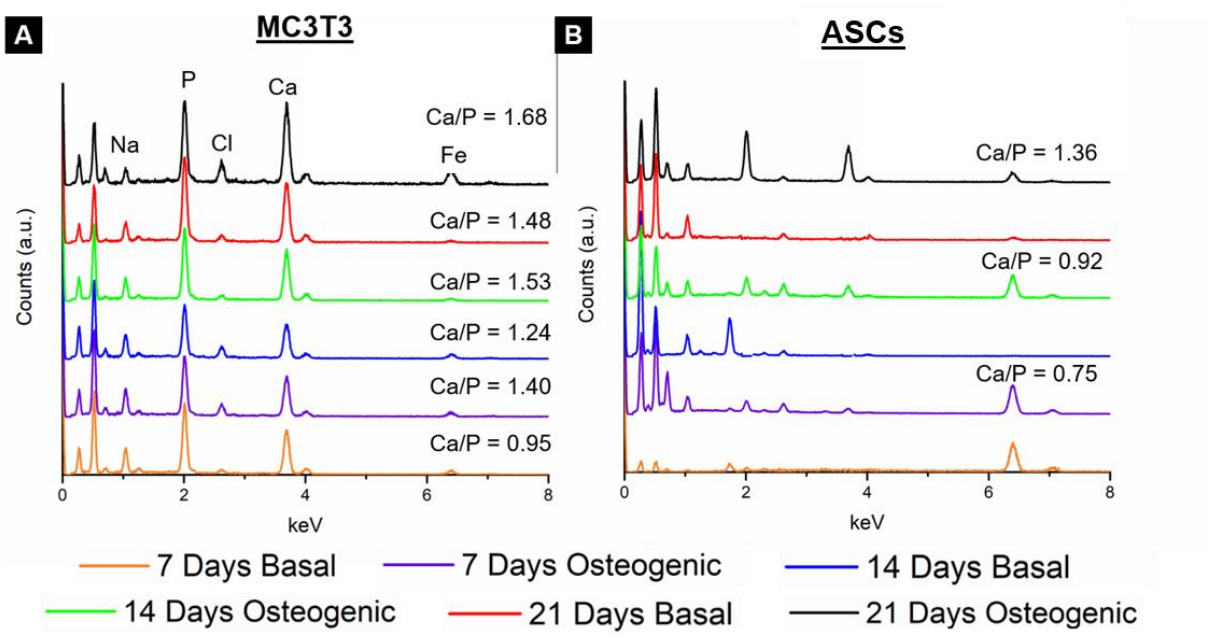

Figure S9. Energy dispersive X-ray spectroscopy (EDS) spectra of deposited minerals in CSs composed by MC3T3-E1 or ASCs after 7, 14 and 21 days in both basal and osteogenic conditions.

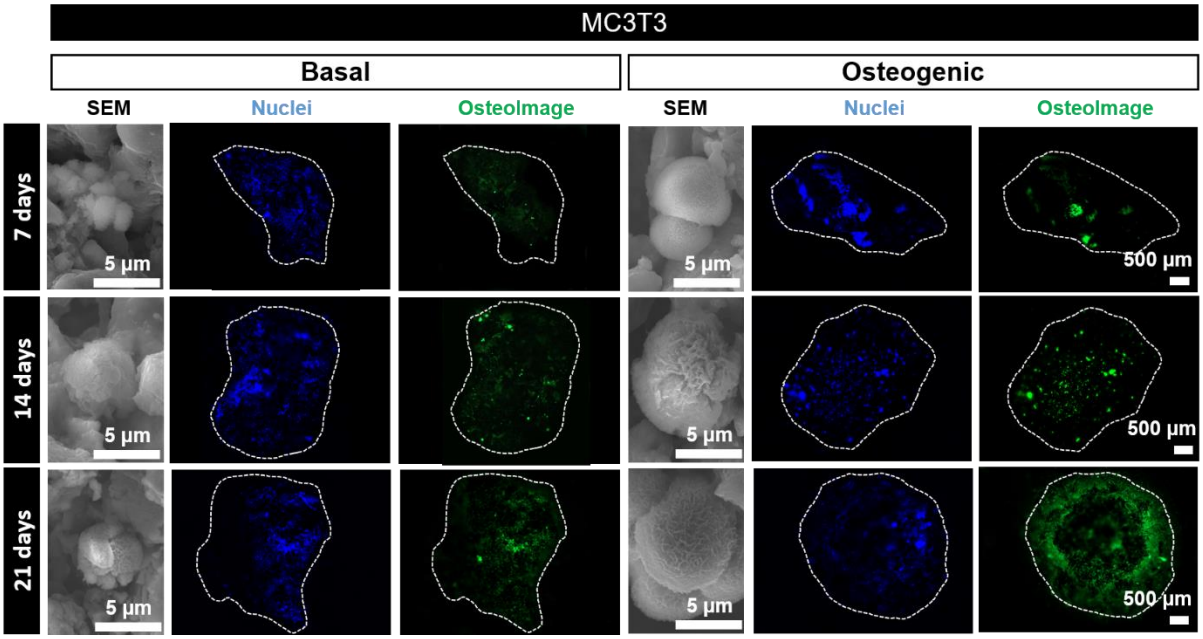

Figure S10. Assessment of the of hydroxyapatite portion of bone-like nodules deposition in MC3T3-homotypic CS through fluorescent OsteoImage^{TM} Mineralization Assay: cell nucleus

- DAPI (blue) and hydroxyapatite (green). Calcium deposits were also identified in SEM micrographs (right panel).

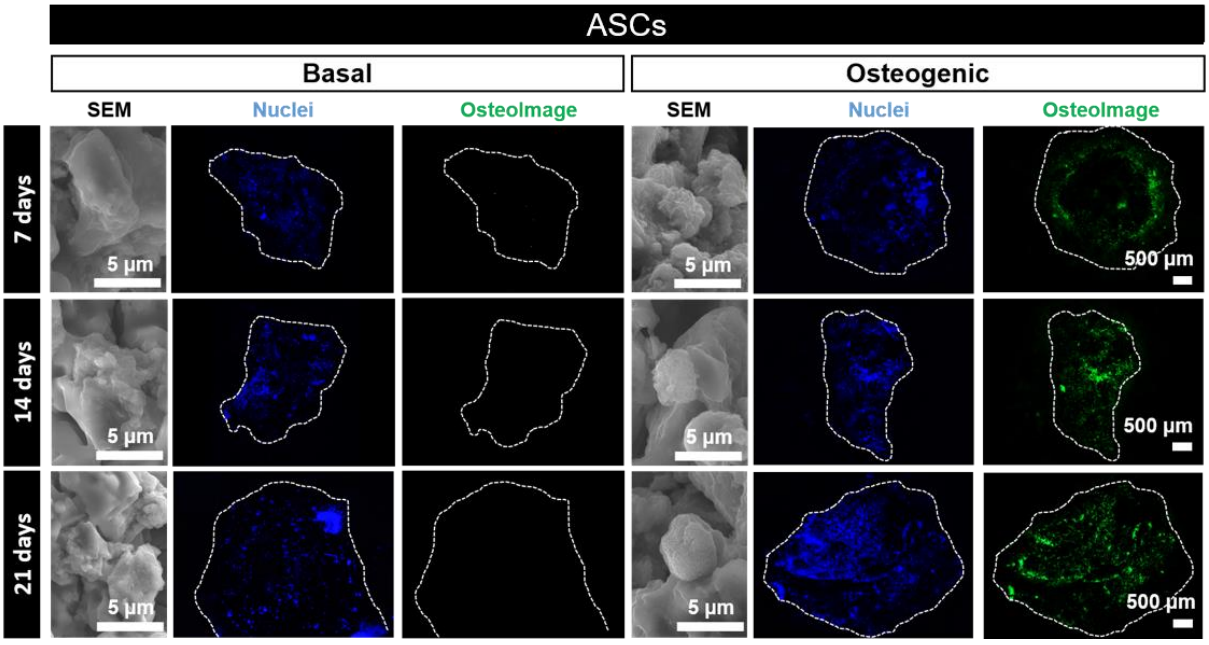

Figure S11. Assessment of the of hydroxyapatite portion of bone-like nodules deposition in ASCs-homotypic CS through fluorescent OsteoImage™ Mineralization Assay: cell nucleus - DAPI (blue) and hydroxyapatite (green). Calcium deposits were also identified in SEM micrographs (right panel).

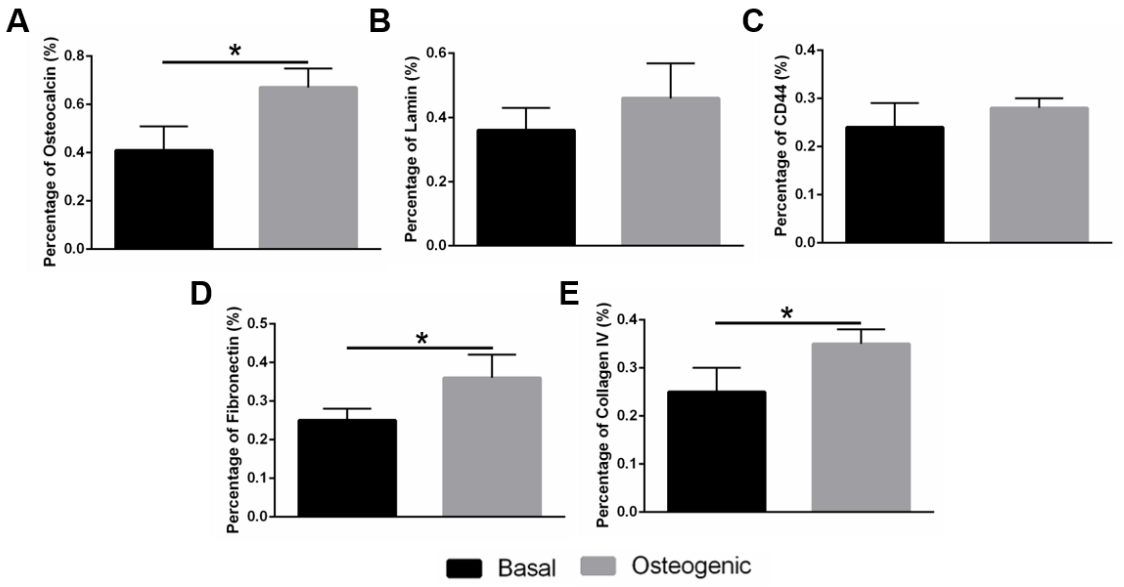

Figure S12: Percentage of osteocalcin (**A**), lamin (**B**), CD44 (**C**), fibronectin (**D**) and collagen IV (**E**) in the representative histological cuts (displayed in Figure 6) of CSs cultured in basal and osteogenic conditions.